Mechanisms of production of hypernuclei in nuclear reactions*

Nihal Buyukcizmeci
Selcuk University, Department of Physics, 42079, Campus, Konya, Turkey

(in collaboration with)
A.S. Botvina, M. Bleicher, A. Ergun, R. Ogul, J. Pochodzalla

January 20, 2016

Workshop on "Production and study of neutron-rich hypernuclei.
Physics and potentialities at FAIR/R3B"
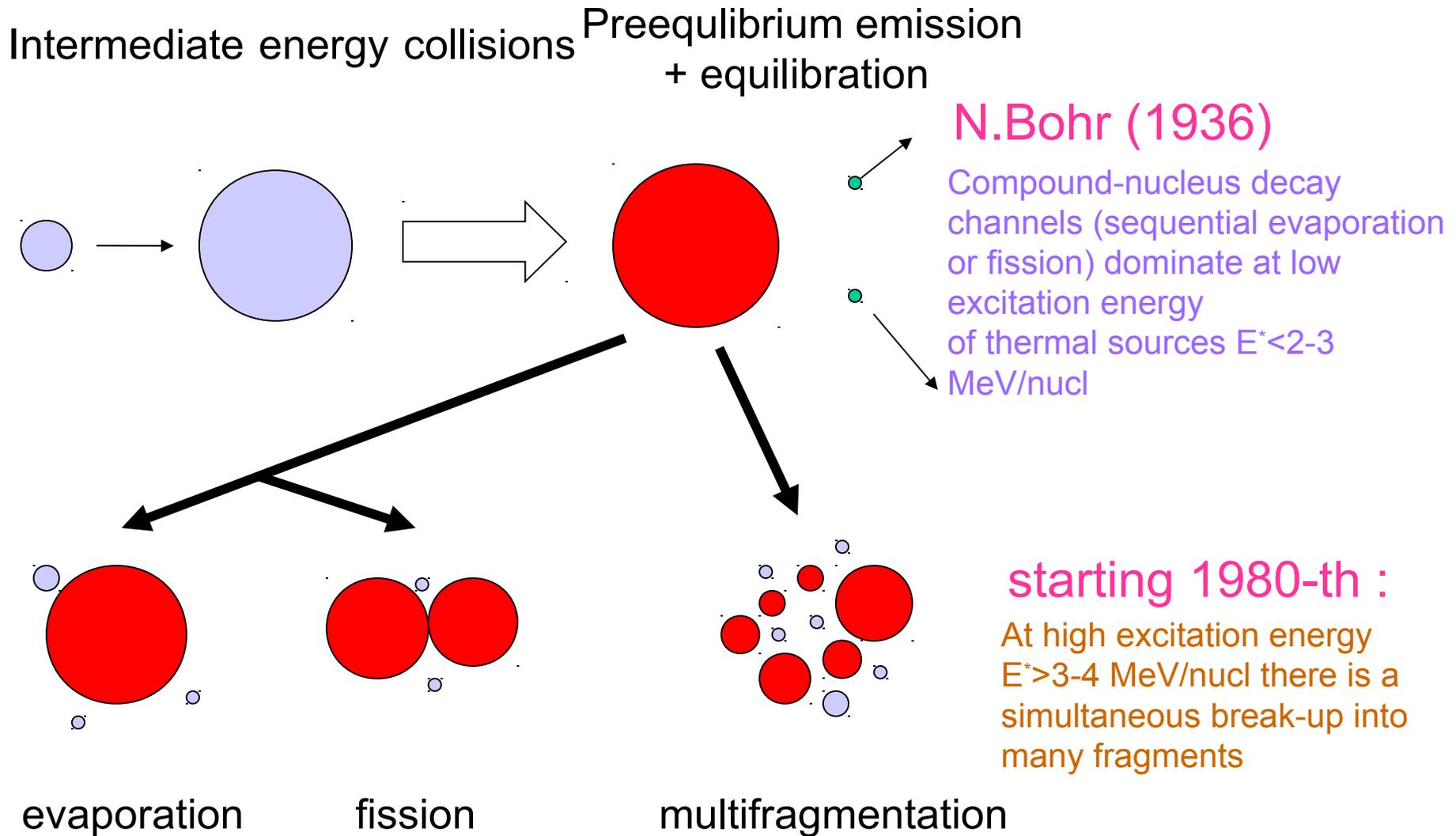Espace de Structure et de réactions Nucléaires Théorique (ESNT)
CEA, SPhN, Orme des Merisiers, France

CONTENT
1. Introduction: Statistical approach, fission, evaporation, fermi break-up, multifragmentation
2. Application of statistical approach for the formation of hyper nuclei : hyper-SMM
3. Investigation of fission and evaporation processes for $\lambda=1$
4. Conclusions

Statistical approach in nuclear reactions: conception of equilibrium

Intermediate energy collisions

Preequlibrium emission + equilibration

N.Bohr (1936)

Compound-nucleus decay channels (sequential evaporation or fission) dominate at low excitation energy of thermal sources $E^* < 2-3$ MeV/nucl

starting 1980-th :

At high excitation energy $E^* > 3-4$ MeV/nucl there is a simultaneous break-up into many fragments

evaporation   fission   multifragmentation

V.Weisskopf (1937) N.Bohr, J.Wheeler (1939) Bondorf et al. (1995) SMM

4.3.3 Evaporation from hot fragments

The successive particle emission from hot primary fragments with A>16 is assumed to be their basic de-excitation mechanism. Due to the high excitation energy of these fragments, standard Weisskopf evaporation scheme [2] was modified to take into account the heavier ejectiles up to ^{18}O, besides light particles (nucleons, d, t, α), in ground and particle-stable excited states [81]. This corresponds to the excitation energies $\varepsilon^{(i)}$ of the ejectiles not higher than 7-8 MeV. By analogy with standard model the width for the emission of a particle j from the compound nucleus (A,Z) is given by:

$$\Gamma_j = \sum_{i=1}^{n} \int_{0}^{E^*_{AZ} - B_j - \varepsilon_j^{(i)}} \frac{\mu_j g_j^{(i)}}{\pi^2 \hbar^3} \sigma_j(E) \frac{\rho_{A'Z'}(E^*_{AZ} - B_j - E)}{\rho_{AZ}(E^*_{AZ})} E\, dE \tag{60}$$

Here the sum is taken over the ground and all particle-stable excited states $\varepsilon_j^{(i)}$ (i=0,1,...n) of the fragment j, $g_j^{(i)} = (2s_j^{(i)}+1)$ is the spin degeneracy factor of the ith excited state, μ_j and B_j are corressponding reduced mass and seperation energy, E^*_{AZ} is the excitation energy of the initial nucleus (55), E is the kinetic energy of an emitted particle in the centre of mass frame. In Eq. (60) ρ_{AZ} and $\rho_{A'Z'}$ are the level densities of the initial (A,Z) and final (A',Z') compound nuclei. They are calculated using the Fermi-gas formula (41). The cross section $\sigma_j(E)$ of the inverse reaction (A',Z')+j=(A,Z) was calculated using the optical model with nucleus-nucleus potential from Ref.[117]. The evaporational process was simulated by the Monte Carlo method using the algorithm described in Ref.[118]. The conservation of energy and momentum was strictly controlled in each emission step.
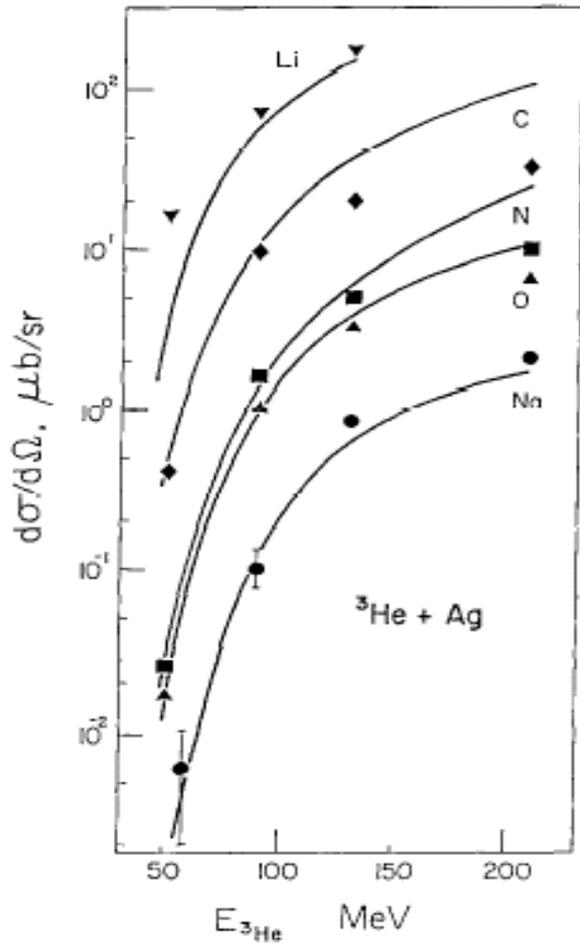
4.3.4. Nuclear fission

An important channel of de-excitation of heavy nuclei (A>200) is fission. This process competes with particle emission. Following the Bohr-Wheeler statistical approach we assume that the partial width for the compound nucleus fission is propotional to the level density at the saddle point $\rho_{sp}(E)$ [1]:

$$\Gamma_f = \frac{1}{2\pi \rho_{AZ}(E^*_{AZ})} \int_0^{E^*_{AZ} - B_f} \rho_{sp}(E^*_{AZ} - B_f - E)\, dE, \qquad (61)$$

Where B_f is the height of the fission barrier which is determined by the Myers-Swiatecki prescription [120]. For approximation of ρ_{sp} we used the results of the extensive analysis of nuclear fissibility and Γ_s/Γ_f branching ratios [121]. The influence of the shell structure on the level densities ρ_{sp} and ρ_{AZ} is disregarded since in the case of multifragmentation we are dealing with very high excitation energies E*>30-50 MeV when shell effects are expected to be washed out [122].
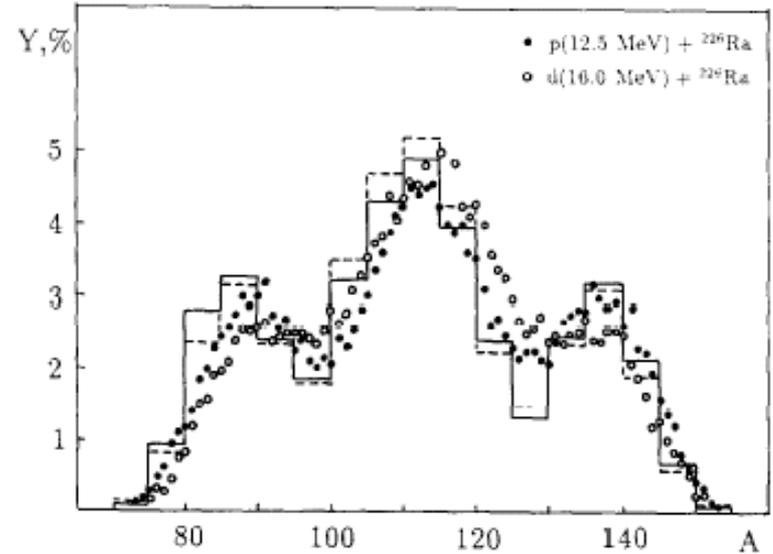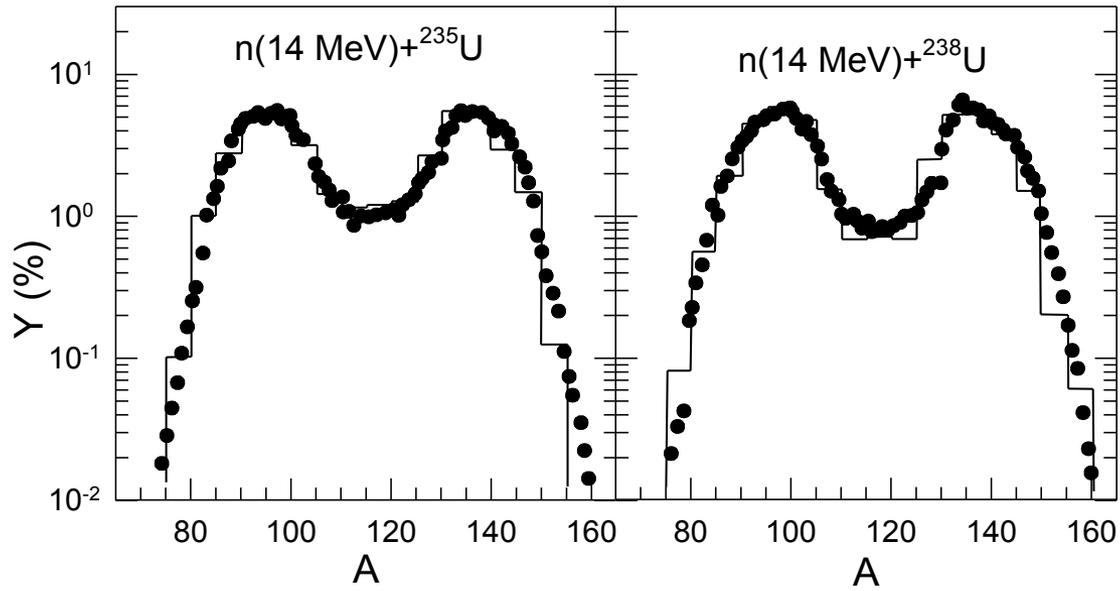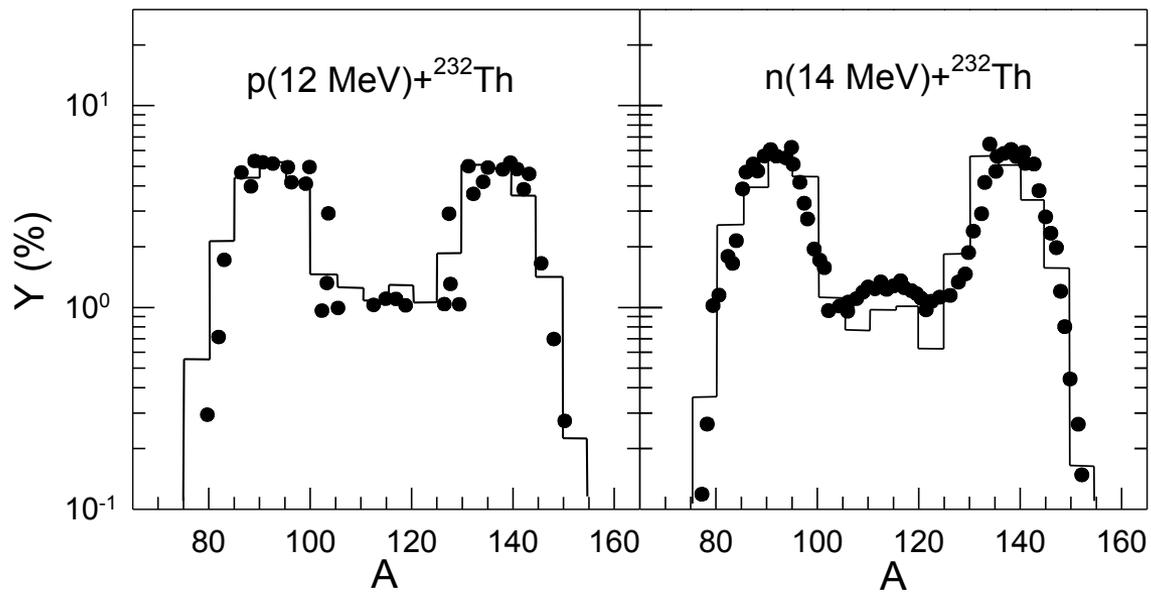
Fig. 4.1. Cross section for heavy cluster emission at backward angles (θ=120-160°) in the reaction ^{3}He+Ag as a function of the laboratory kinetic energy of ^{3}He. The data are from Ref.[119], and the curves show the results of the evaporation model calculation described in the text.
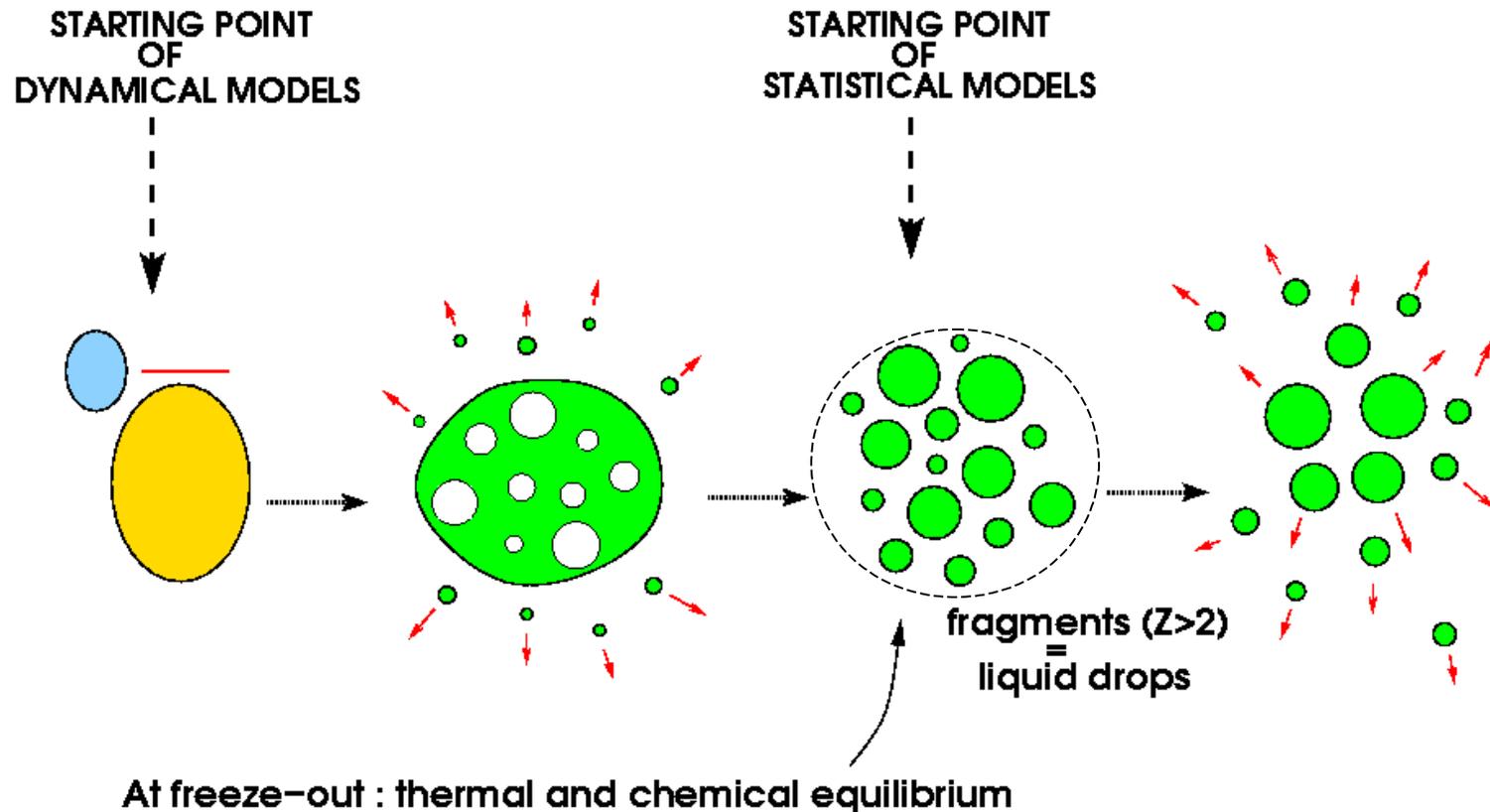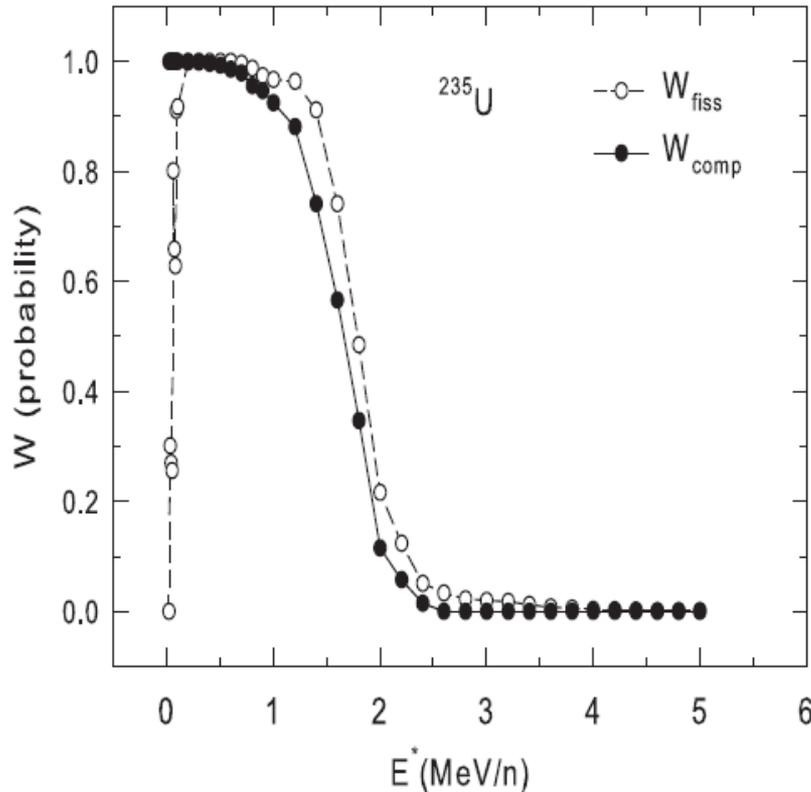
Nuclear fission

# Multifragmentation in intermediate and high energy nuclear reactions

Experimentally established:

1) few stages of reactions leading to multifragmentation,

2) short time ~100fm/c for primary fragment production,

3) freeze-out density is around $0.1\rho_0$,

4) high degree of equilibration at the freeze-out,

5) primary fragments are hot.

STARTING POINT
OF
DYNAMICAL MODELS

STARTING POINT
OF
STATISTICAL MODELS

fragments (Z>2)
=
liquid drops

At freeze−out : thermal and chemical equilibrium

Survival probability of the compound nucleus Wcomp and fission probability Wfiss as a function of the excitation energy, for the disintegration of ^{235}U as obtained in the present SMM calculations.
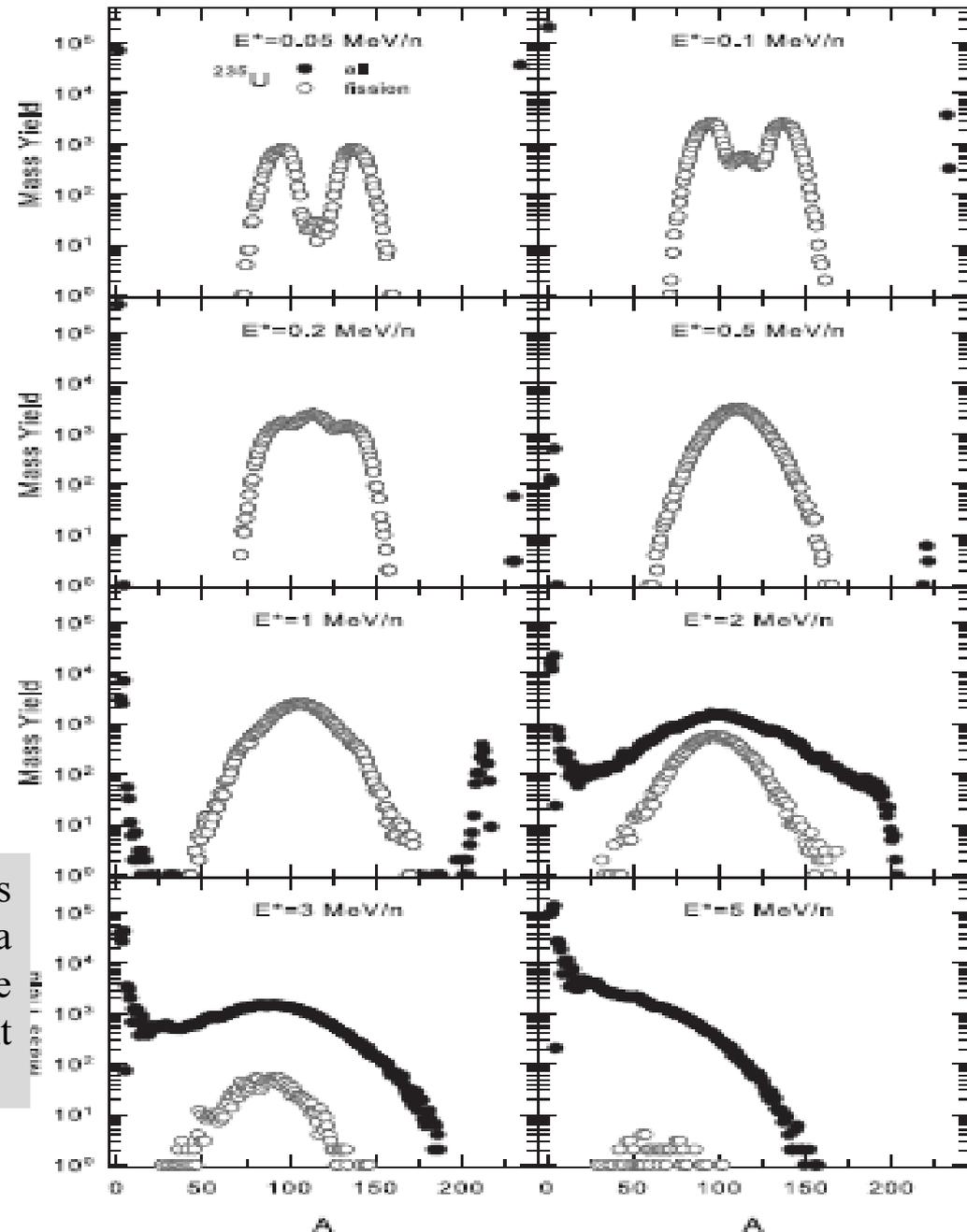
MULTICS

Au(35MeV/N)+Au, peripheral
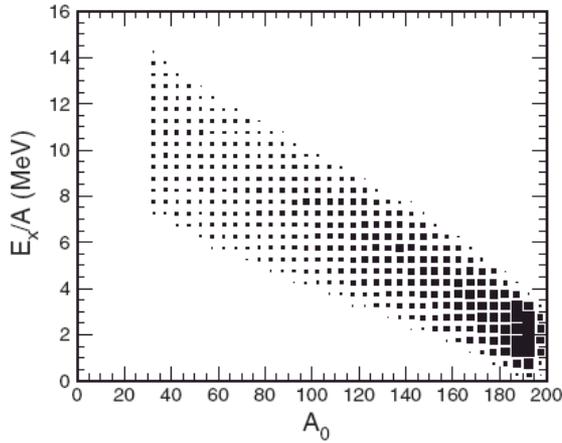
2 MeV/n →
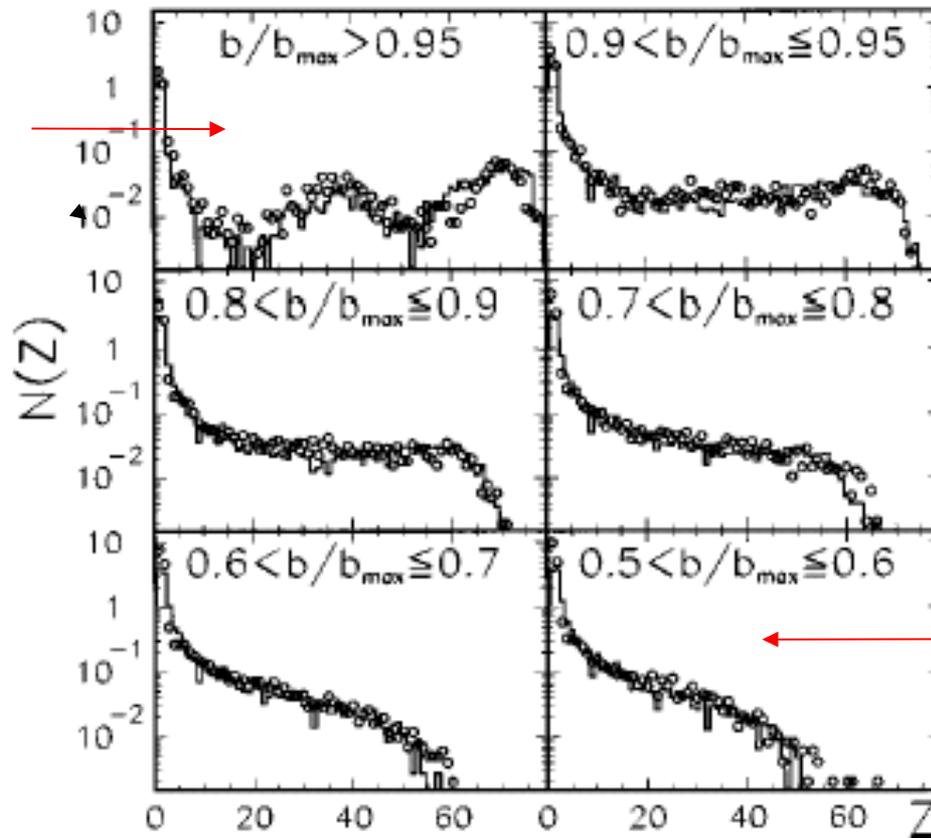
← **5 MeV/n**

Fig.8. Charge distributions for peripheral and midperipheral collisions

(open point:experimental data; histogram:SMM predictions).
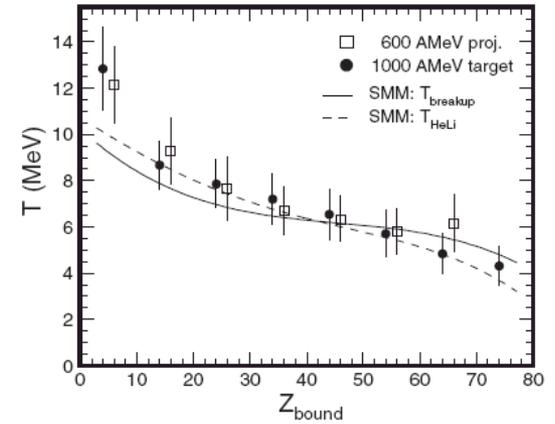
ALADIN data

GSI

multifragmentation of relativistic projectiles

A.S.Botvina et al.,
Nucl.Phys. A584(1995)737
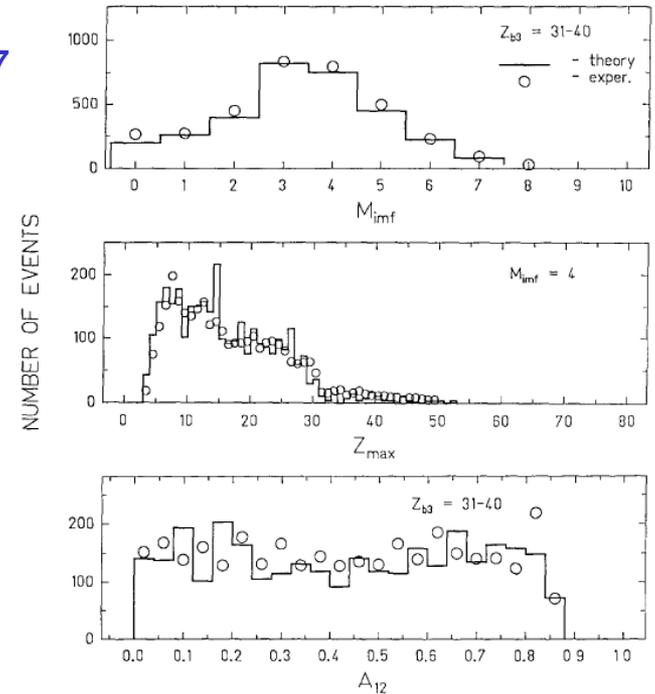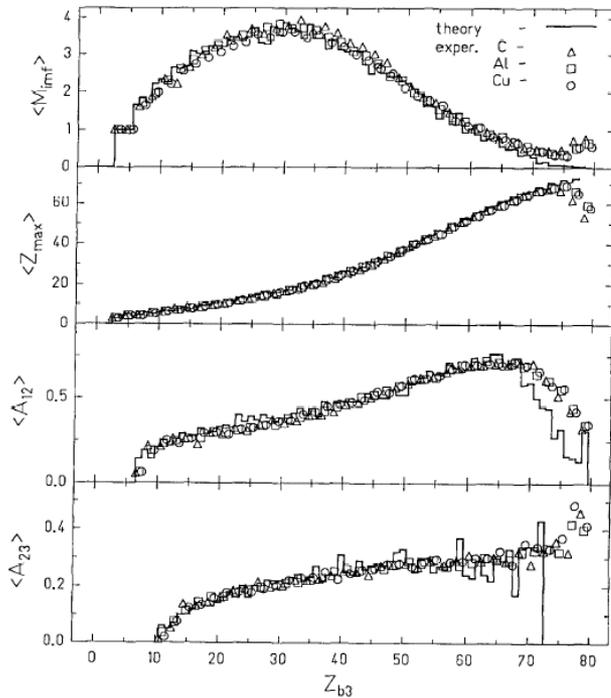
H.Xi et al.,
Z.Phys. A359(1997)397

comparison with SMM (statistical multifragmentation model)

Statistical equilibrium has been reached in these reactions
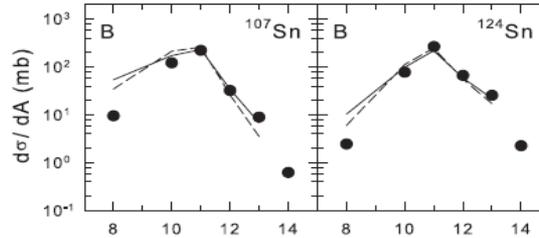

Au(600 MeV/n) + C, Al, Cu

Au(600 MeV/n) + Cu

Isospin-dependent multifragmentation of relativistic projectiles

124,107-**Sn**, 124-**La** (600 A MeV) + **Sn** → projectile (multi-)fragmentation

Very good description is obtained within Statistical Multifragmentation Model, including fragment charge yields, isotope yiels, various fragment correlations.
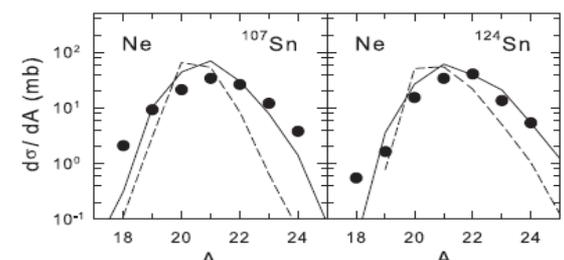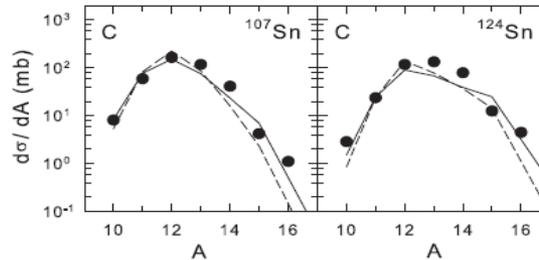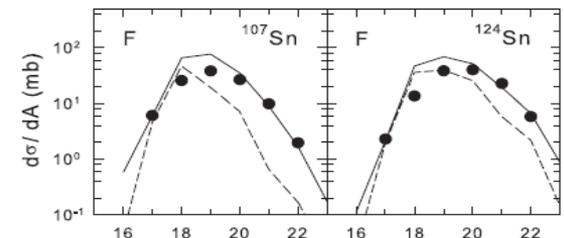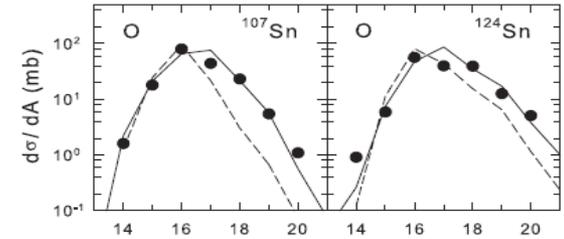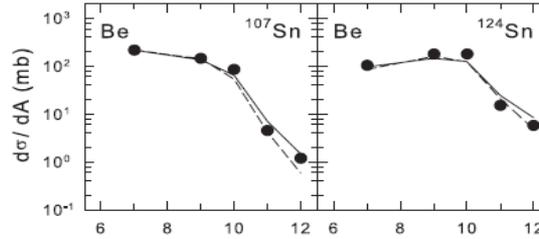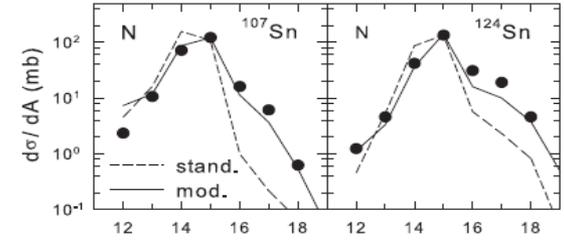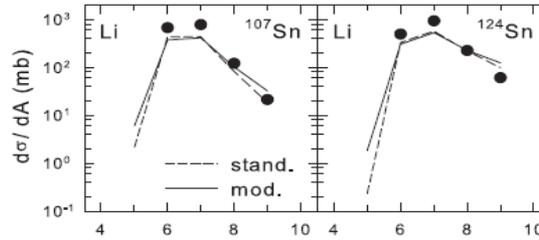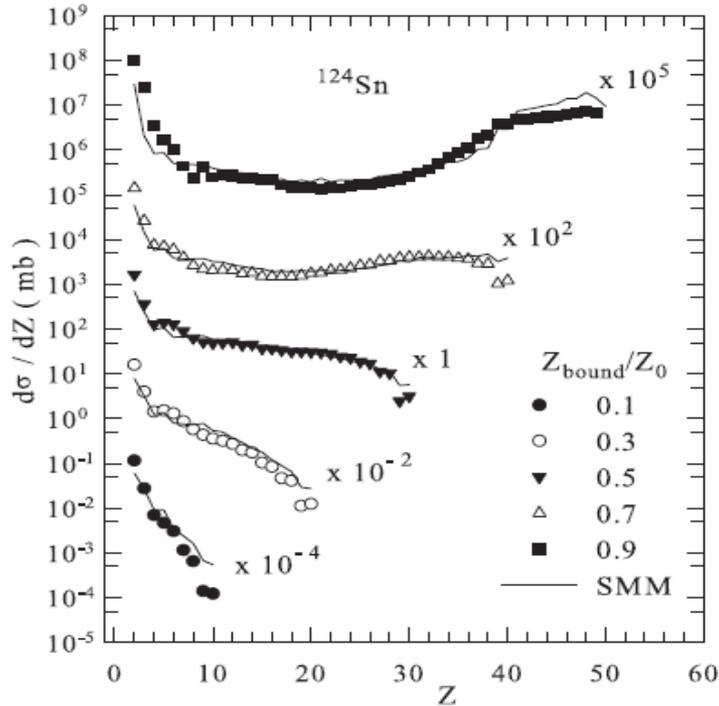
Statistical (chemical) equilibrium is established at break-up of hot projectile residues ! In the case of strangeness admixture we expect it too !

Two-stage multifragmentation of 1A GeV Kr, La, and Au
J. A. Hauger et al. Phys. Rev. C **62**, 024616 (2000)
EOS collaboration

Fig. 19. Caloric curves (Tf vs E^*_{th}/A) for Kr, La and, Au. Points are experimental and curves are from SMM.

Fig.24. Second stage fragment charge distribution as a function of Z/Zprojectile. Results are shown For three reduced multiplicity intervals for both data and SMM.

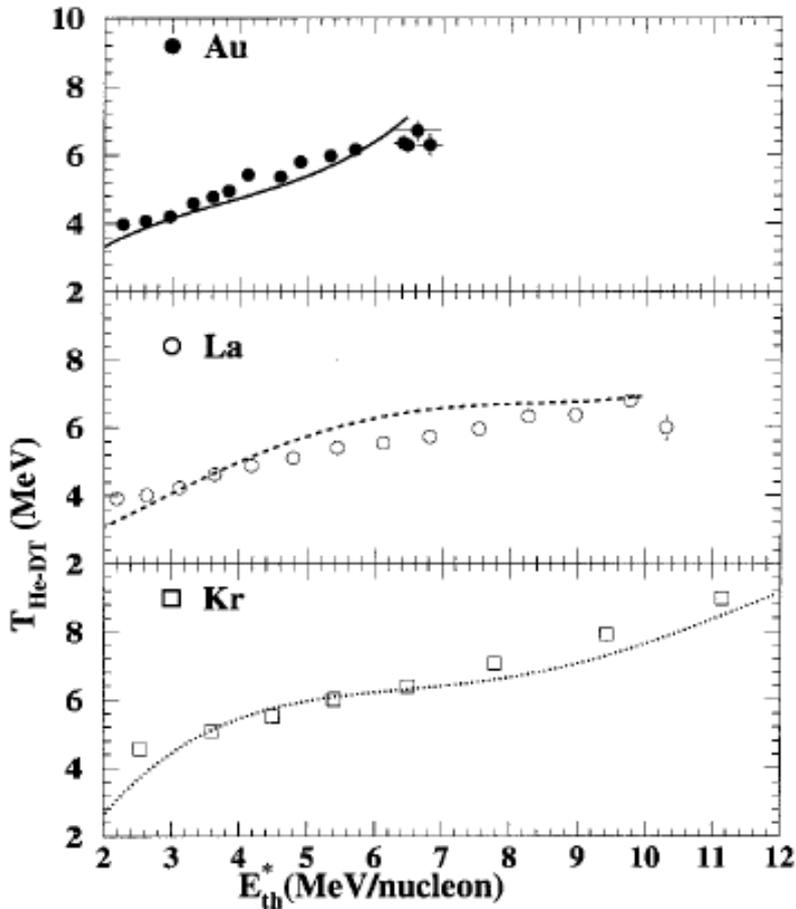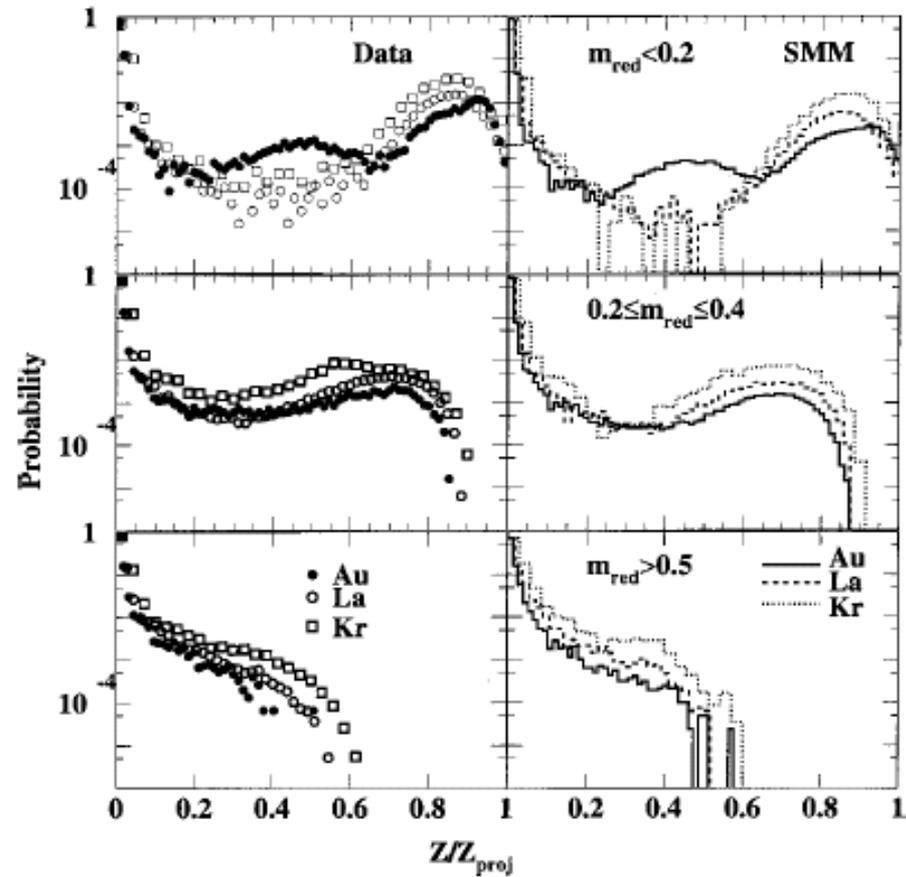# FRS data @ GSI

FRS projectile fragmentation of two symetric systems ^{124}Sn + ^{124}Sn and ^{112}Sn + ^{112}Sn at an incident beam energy of 1 A GeV measured with high-resolution magnetic spectrometer FRS
(V. Föhr, et al., Phys. Rev. **C 84**, (2011) 054605)

Experimental data are well reproduced with statistical calculations in the SMM–ensemble .
To reproduce the FRS data symmetry energy term is reduced as shown in the table.
We have also found a decreasing trend of the symmetry energy with increasing charge number, for the neutron-rich heavy fragments resulting from ^{124}Sn projectile.
H. Imal, A.Ergun, N. Buyukcizmeci, R.Ogul, A.S. Botvina, W. Trautmann, C **91**, 034605 (2015)

Z interval	^{112}Sn γ(MeV)	^{124}Sn γ (MeV)
10-17	16	16
18-25	19	18
26-31	21	20
32-37	23	19
38-45	25	18
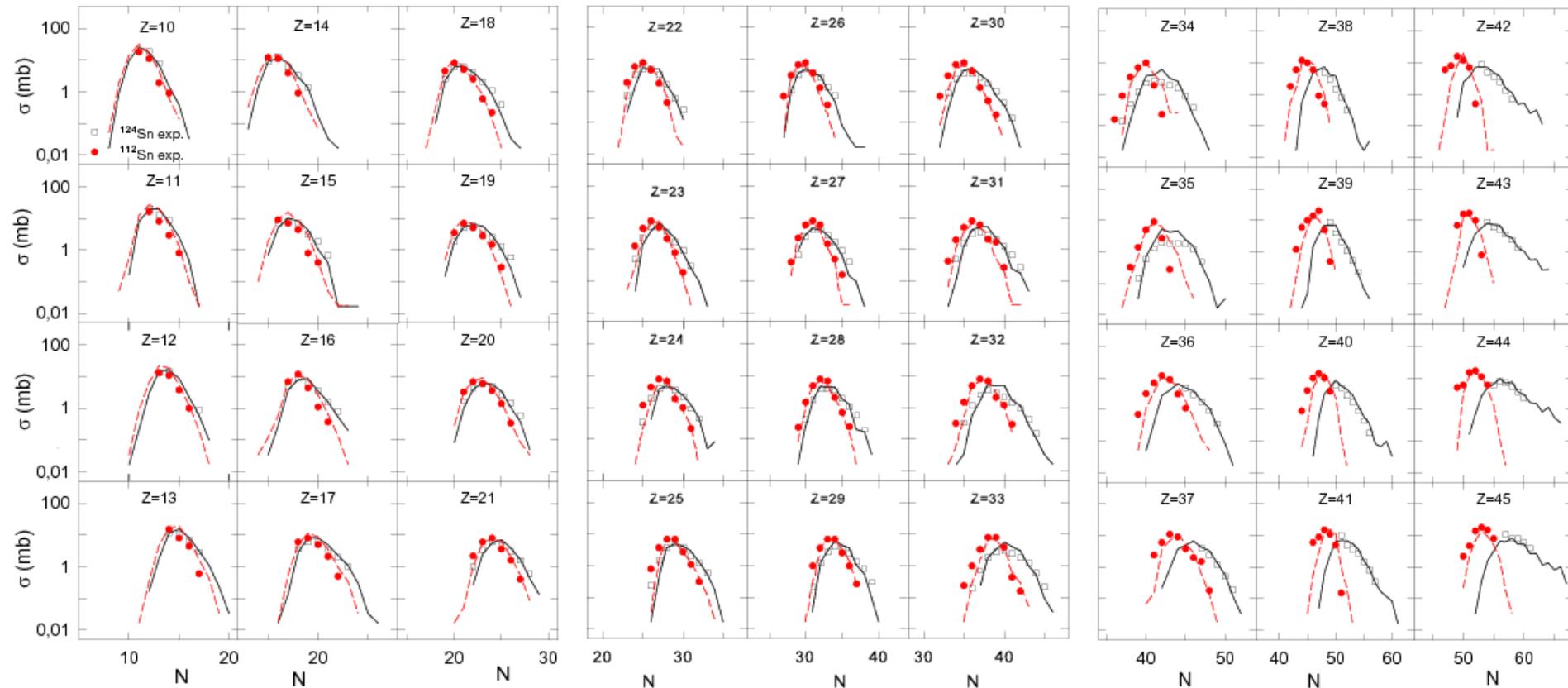
Multifragmentation versus sequential evaporation

ISIS   π⁻(8GeV/c)+Au

ALADIN   Au (600 MeV/n) +X.

FIG. 3. Left panel: dots present the raw measured probability to detect an event with at least one heavy-fragment, $Z \geqslant 8$, and solid (dotted) line presents the SMM (GEMINI) model prediction filtered with t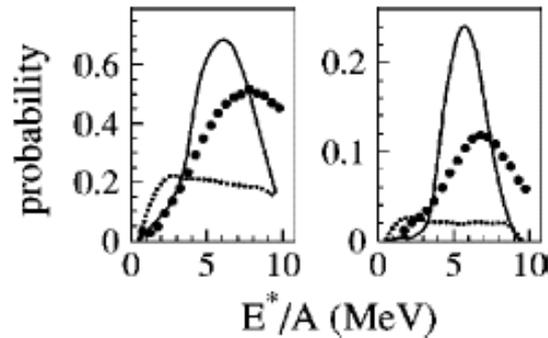he experimental detection efficiency. An initial angular momentum of $L = 20\hbar$ for the hot nucleus was assumed for GEMINI model calculations. Right panel: as in left panel, but for the probability of detecting events with at least two heavy-fragments, $Z \geqslant 8$.
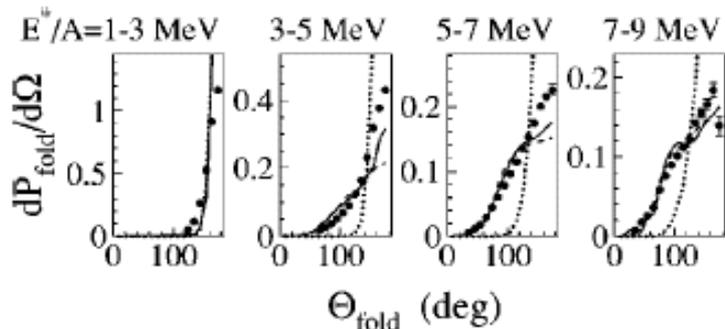
FIG. 2. The measured folding-angle (the angle between two $Z \geqslant 8$ fragments) probability for the indicated excitation-energy bins. Solid, dashed, and dotted lines show the SMM-hot, SMM-cold, and GEMINI model predictions, respectively, filtered with the experimental detection efficiency.

Fig. 15. The average multiplicity of IMFs as a function of Z_{bound} for Au 600 MeV/nucleon collisions on C (circles), Al (triangles), Cu (squares) and Pb (stars). The error bars are in most cases smaller than the size of the symbols. The lines are COPENHAGEN (dashed), GEMINI (dotted) and percolation (full) predictions.

4.3.2. The Fermi break-up

For light primary fragments (with $A \leq 16$) even a relatively small excitation energy may be comparable with their total binding energy. In this case we assume that the princip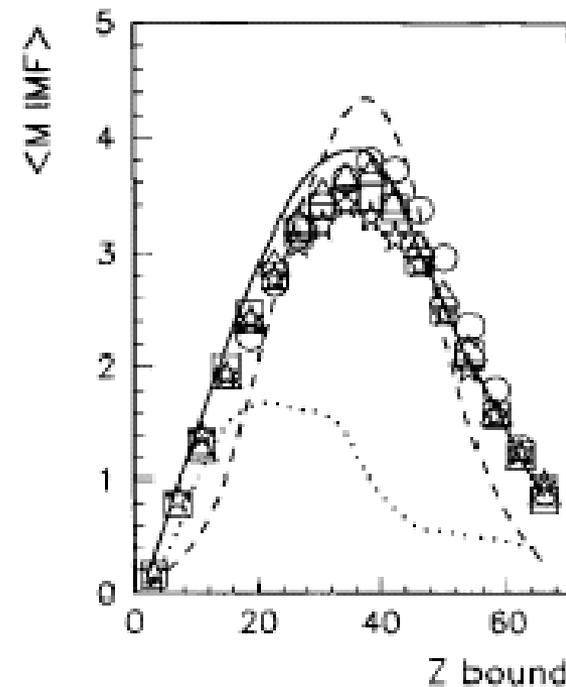al mechanism of de-excitation is the explosive decay of the excited nucleus into several smaller clusters (the secondary break-up). To describe this process we use the famous Fermi model [105]. It is analogous to the above-described statistical model, but all final-state fragments are assumed to be in their ground or low excited states. In this case the statistical weight of the channel containing n particles with masses m_i $(i = 1, \ldots, n)$ in volume V_f may be calculated in microcanonical approximation:

$$\Delta \Gamma_f^{\text{mic}} \propto \frac{S}{G} \left(\frac{V_f}{(2\pi\hbar)^3} \right)^{n-1} \left(\frac{\prod_{i=1}^{n} m_i}{m_0} \right)^{3/2} \frac{(2\pi)^{(3/2)(n-1)}}{\Gamma(\frac{3}{2}(n-1))} \left(E_{\text{kin}} - U_f^C \right)^{(3/2)n-5/2}, \tag{58}$$

where $m_0 = \sum_{i=1}^{n} m_i$ is the mass of the decaying nucleus, $S = \prod_{i=1}^{n}(2s_i + 1)$ is the spin degeneracy factor (s_i is the ith particle spin), $G = \prod_{j=1}^{k} n_j!$ is the particle identity factor (n_j is the number of particles of kind j). E_{kin} is the total kinetic energy of particles at infinity which is related to the prefragment excitation energy E_{AZ}^* as

$$E_{\text{kin}} = E_{AZ}^* + m_0 c^2 - \sum_{i=1}^{n} m_i c^2. \tag{59}$$

U_f^C is the Coulomb interaction energy between cold secondary fragments given by Eq. (49), U_f^C and V_f are attributed now to the secondary break-up configuration.

$$\Omega = \int \frac{V^M \, \mathrm{d}^3 p_1 \cdots \mathrm{d}^3 p_M}{(2\pi\hbar)^{3M}} \delta \left(\sum_{A,Z} p_{AZ} \right) \delta \left(\sum_{A,Z} \frac{p_{AZ}^2}{2m_{AZ}} - \sum_{A,Z} E_{AZ}^{\text{kin}} \right)$$
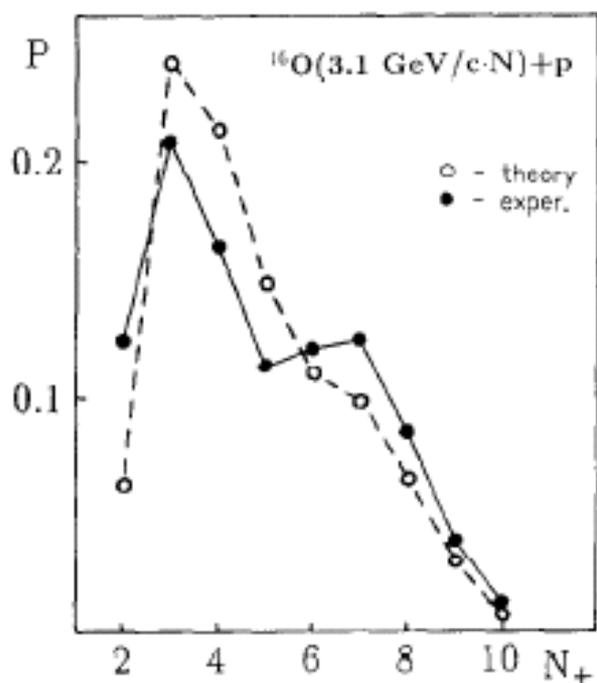
Fermi-break-up for light nuclei

$\pi^- + {}^{12}C$ at rest

Fig. 6.13. Energy spectra of He and Li fragments produced after absorption of stopped π^--mesons in ${}^{12}C$ nucleus. The detected particles are indicated in the figure. The histograms are calculated as described in the text. The experimental data: solid curves [160], dashed curves [161], dots [162].

Fig. 6.12. Multiplicity distribution of positively charged particles N_+ produced in ${}^{16}O(3.1$ GeV/c per nucleon$) + p$ reaction. The dots are experimental data from [159]. The open circles are the CFEM calculation.

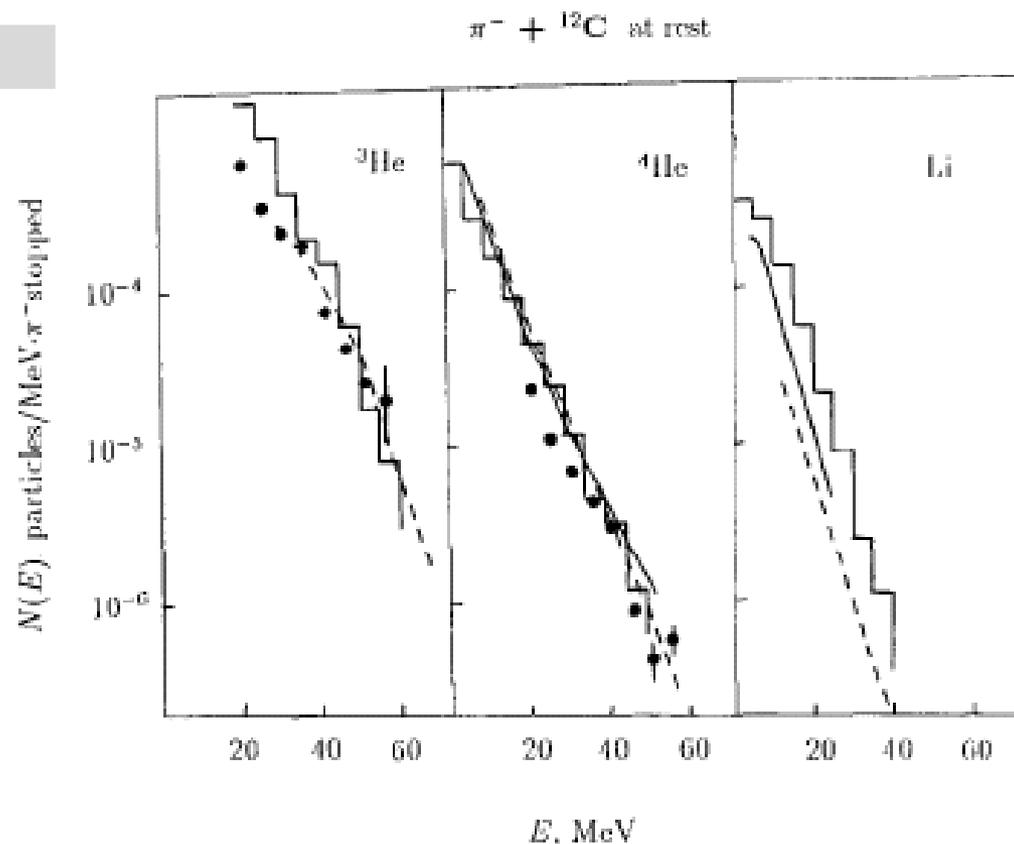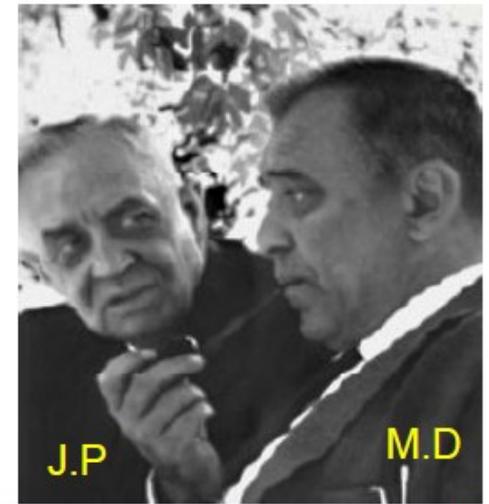# Discovery of a Strange nucleus: Hypernucleus
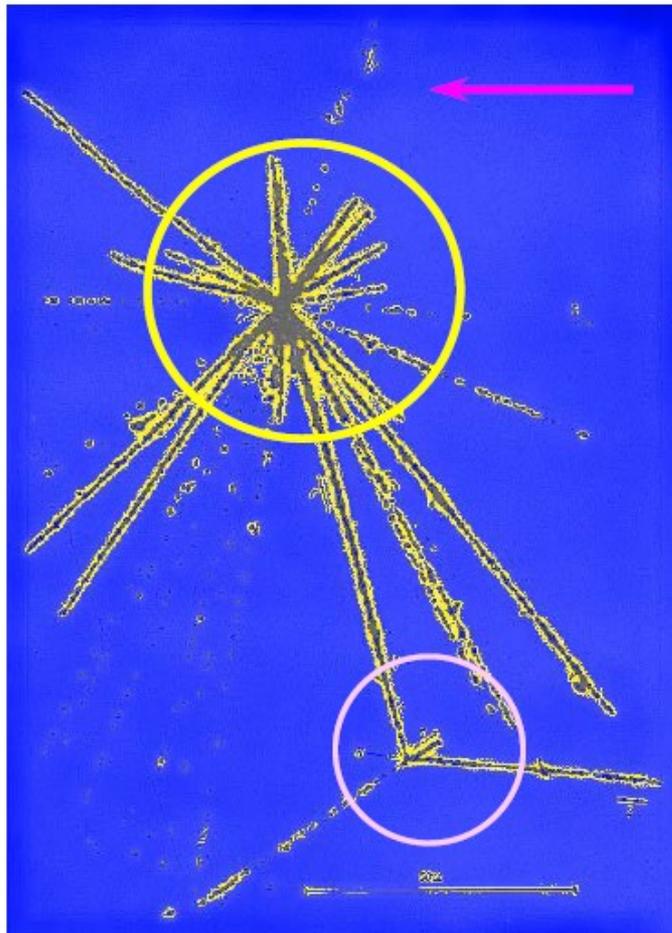
M. Danysz and J. Pniewski, Philos. Mag. 44 (1953) 348

First-hypernucleus was observed in a stack of photographic emulsions exposed to cosmic rays at about 26 km above the ground.

J.P   M.D

Incoming high energy proton from cosmic ray

colliding with a nucleus of the emulsion, breaks it in several fragments forming a star. **Multifragmentation !**

All nuclear fragments stop in the emulsion after a short path

From the first star, 21 Tracks => $9\alpha + 11H + 1\ _\Lambda X$

The fragment $_\Lambda X$ disintegrates later , makes the bottom star. Time taken ~ 10^{-12} sec (typical for weak decay)

This particular nuclear fragment, and the others obtained afterwards in similar conditions, were called **hyperfragments or hypernuclei.**

Generalization of the statistical de-excitation model for nuclei with Lambda hyperons

In these reactions we expect analogy with

multifragmentation in intermediate and high energy nuclear reactions

+ nuclear matter with strangeness

STARTING POINT
OF
DYNAMICAL MODELS

STARTING POINT
OF
STATISTICAL MODELS

hyperfragments

Λ hyperons captured

fragments (Z>2)
=
liquid drops

production of hypermatter

At freeze−out : thermal and chemical equilibrium
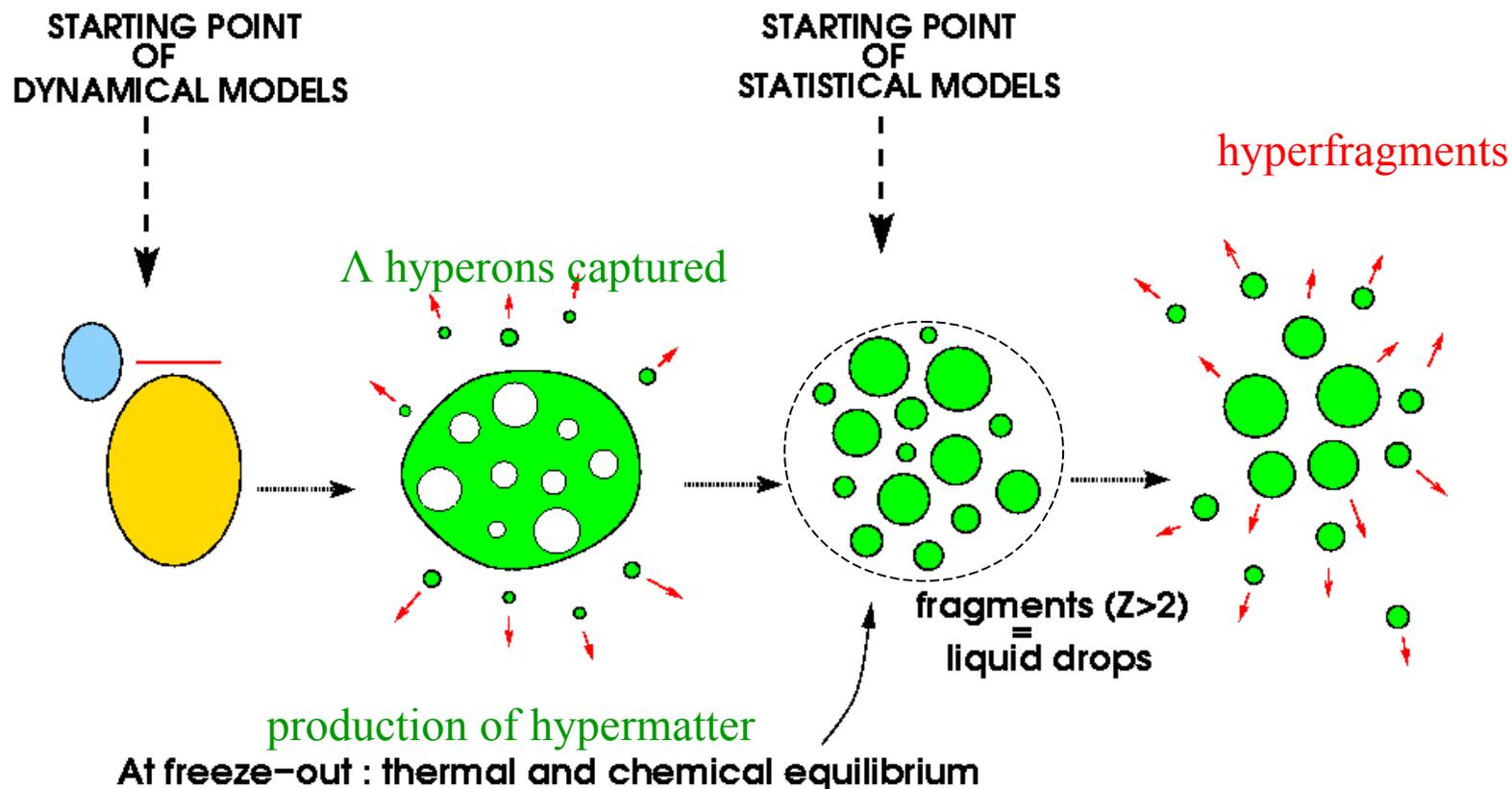
Statistical approach for fragmentation of hyper-matter

$$Y_{\text{AZH}} = g_{\text{AZH}} V_f \frac{A^{3/2}}{\lambda_T^3} \exp\left[-\frac{1}{T}\left(F_{AZH} - \mu_{AZH}\right)\right]$$

mean yield of fragments with mass number A, charge Z, and Λ-hyperon number H

$$\mu_{AZH} = A\mu + Z\nu + H\xi$$

$$F_{AZH}(T,V) = F_A^B + F_A^S + F_{AZH}^{\text{sym}} + F_{AZ}^C + F_{AH}^{\text{hyp}}$$

liquid-drop description of fragments: bulk, surface, symmetry, Coulomb (as in Wigner-Seitz approximation), and hyper energy contributions
J.Bondorf et al., Phys. Rep. **257** (1995) 133

$$F_A^B(T) = \left(-w_0 - \frac{T^2}{\varepsilon_0}\right) A \;,$$

$$F_A^S(T) = \beta_0 \left(\frac{T_c^2 - T^2}{T_c^2 + T^2}\right)^{5/4} A^{2/3} \;,$$

parameters $\approx$ Bethe-Weizsäcker formula:

$$F_{AZH}^{\text{sym}} = \gamma \frac{(A - H - 2Z)^2}{A - H} \;,$$

$w_0 = 16$ MeV, $\beta_0 = 18$ MeV, $T_c = 18$ MeV

$\gamma = 25$ MeV $\qquad \varepsilon_0 \approx 16$ MeV

$$\sum_{AZH} A Y_{\text{AZH}} = A_0, \quad \sum_{AZH} Z Y_{\text{AZH}} = Z_0, \quad \sum_{AZH} H Y_{\text{AZH}} = H_0.$$

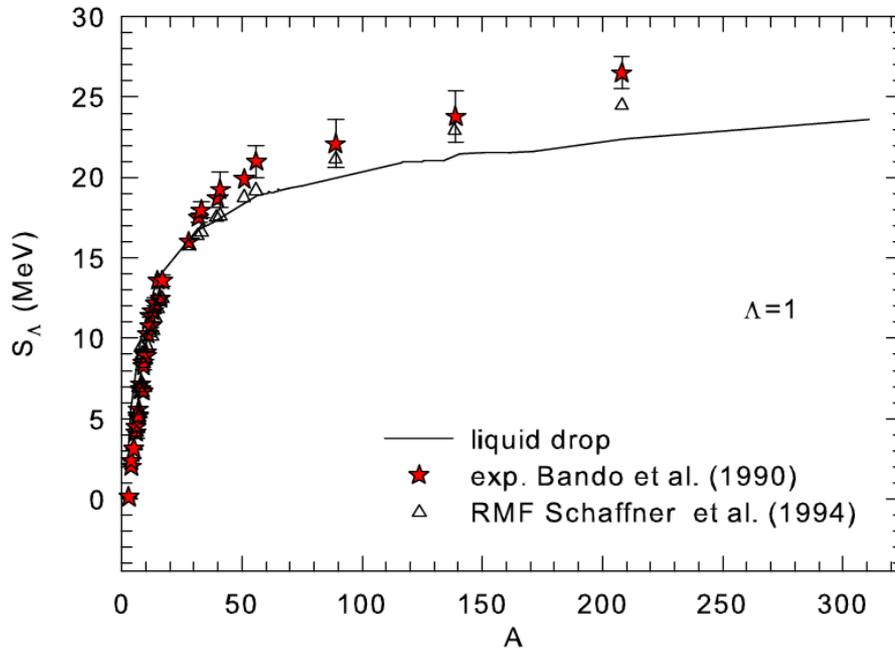chemical potentials are from mass, charge and Hyperon number conservations

$$F_{AH}^{\text{hyp}} = E_{sam}^{\text{hyp}} = H \cdot (-10.68 + 48.7/(A^{2/3})).$$

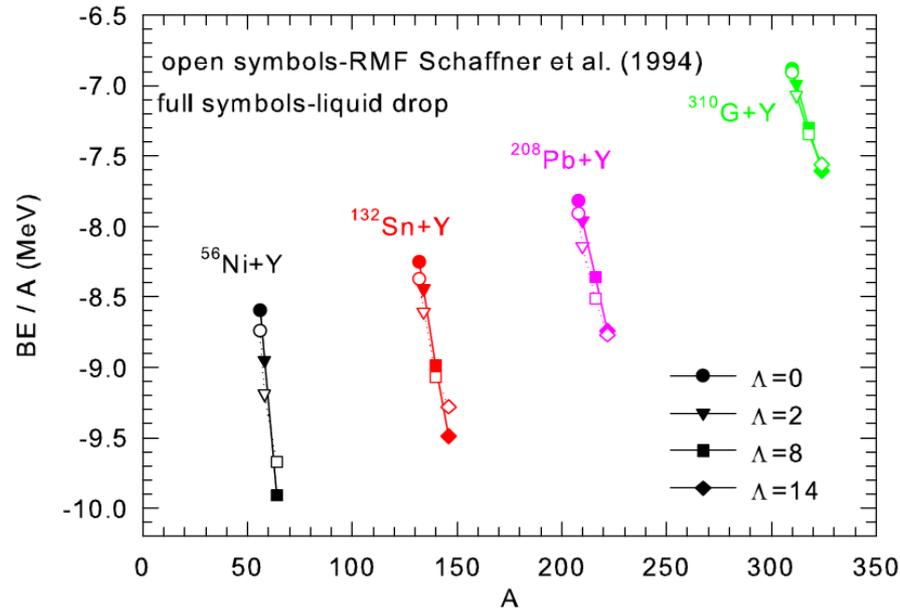-- C.Samanta et al. J. Phys. G: 32 (2006) 363 (motivated: single Λ in potential well)

$$F_{AH}^{\text{hyp}} = (H/A) \cdot (-10.68A + 21.27A^{2/3}).$$

-- liquid-drop description of hyper-matter

Separation energy

Binding energy

liquid-drop approximation

N.Buyukcizmeci et al., PRC88 (2013) 014611

Break-up of excited hyper-residues

Normal nuclei + hypernuclei can be formed via evaporation, fission and multifragmentation processes.

Liquid-gas type phase transition in hyper-matter is expected at subnuclear densities.

Very broad distributions of nuclei similar to ones in normal nuclear matter. At moderate temperatures hyperons concentrate in large species

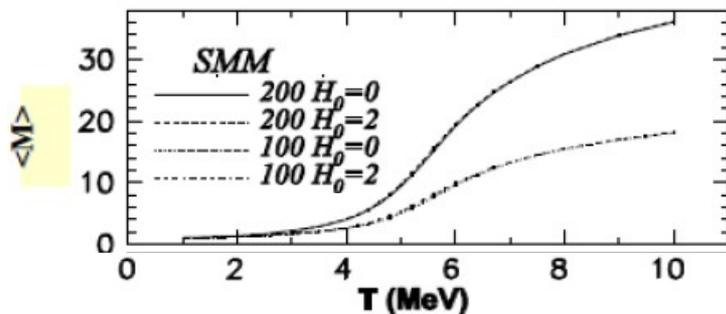Important: formed hypernuclei can reach beyond traditional neutron and proton drip-lines

N.Buyukcizmeci et al., PRC88 (2013) 014611
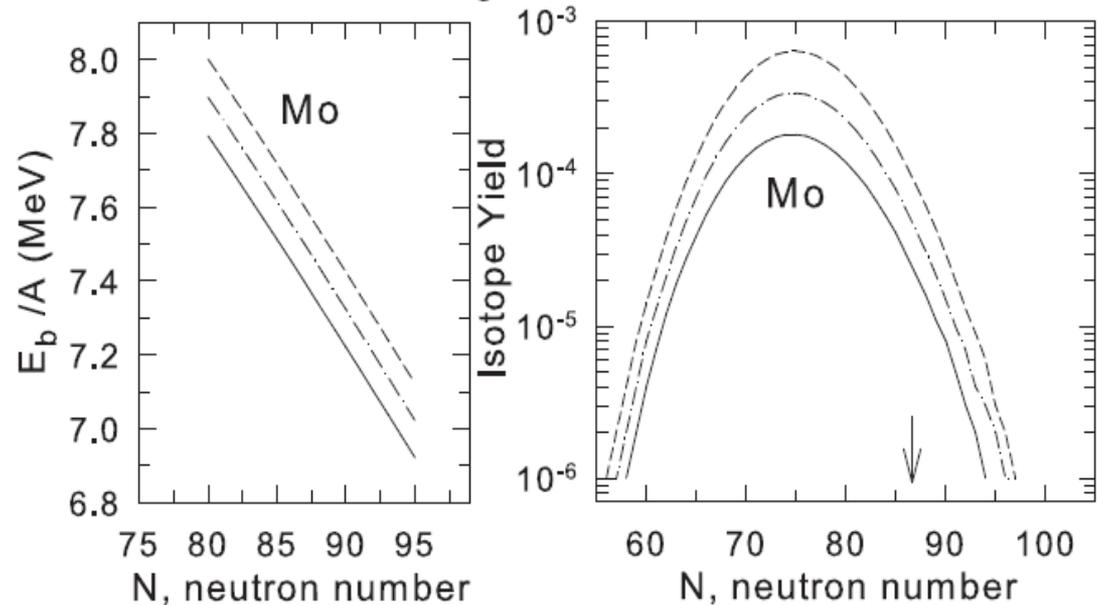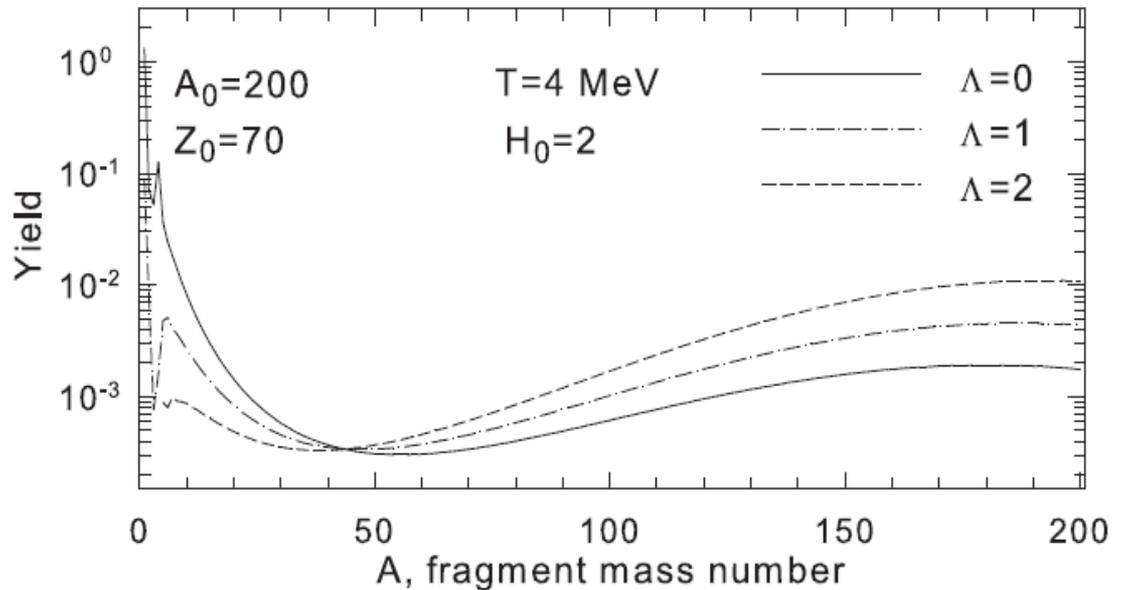
Multifragmentation of excited hyper-sources

H_0 is the number of hyperons in the system

General picture depends weakly on strangeness content (in the case it is much lower than baryon charge)

Mean multiplicity

There are differences in yield of hyper-fragments depending on their properties.
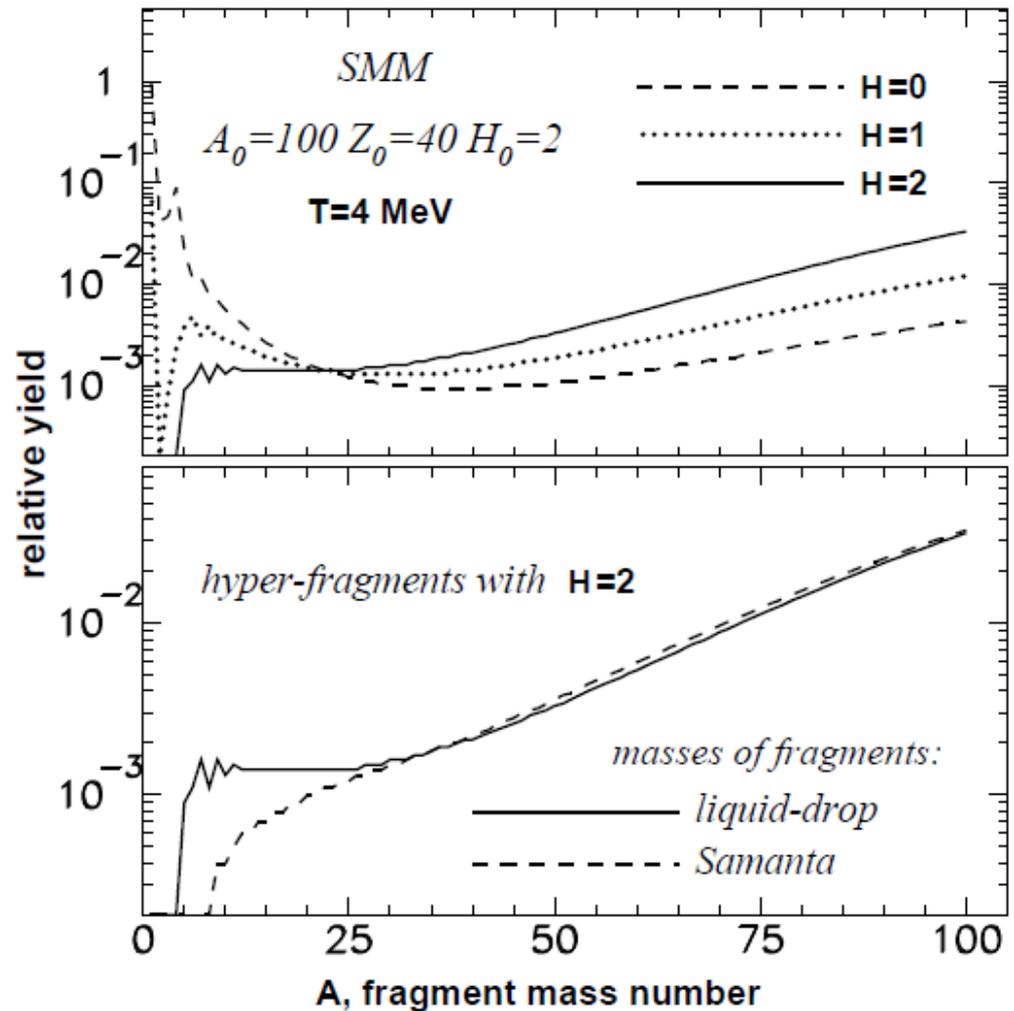

Fig. 3. Multifragmentation of an excited double-strange system with mass number 100 and charge 40, at temperature 4 MeV. Top panel – yield of fragments containing 0, 1, and 2 Λ hyperons. Bottom panel – effect of different mass formulae with strangeness on production of double hyperfragments [13].

A.S.Botvina and J.Pochodzalla, Phys. Rev.C76 (2007) 024909

Toward a fission of low excited hyper-sources

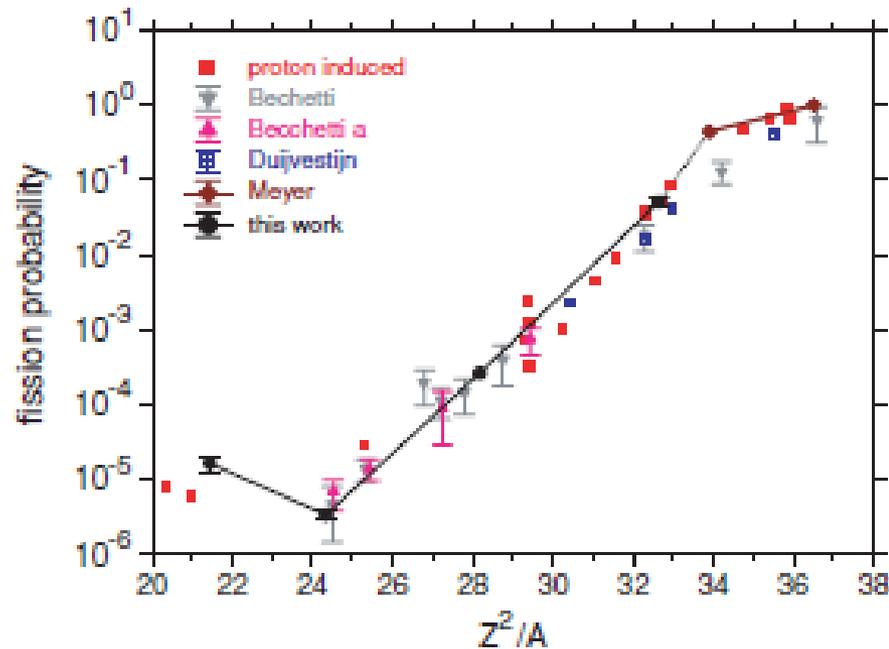## Fission studies with 140 MeV α particles

FIG. 4. (Color online) The fission probability as a function of the fissility parameter. The dots with error bars are the present results and diamonds are from Ref. [21]. The lines are to guide the eye. The squares are for proton-induced fission at energies 150 to 200 MeV [22,23]. The other data shown were measured with 190 MeV protons: triangles down [24], triangles up [25], and those shown by crossed squares were measured by radiochemical methods [26].

Properties of normal fission

TABLE II. Cross section for fission for the different target nuclei. Also given are estimates for the fission barriers obtained by the linear dependence of the fission parameter [denoted by (I)] and on the exponential given in the text [denoted by (II)].

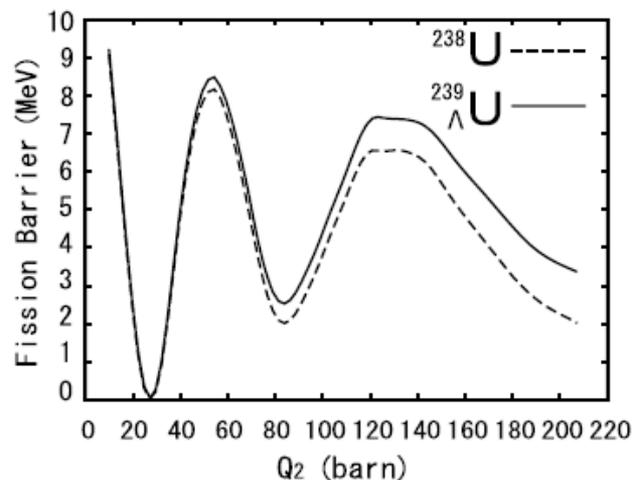| Target	σ_{fiss} (mb)	B_f (MeV) (I)	B_f (MeV) (II)
^{nat}Ag	0.030 ± 0.007	38.8	49.1
^{139}La	0.007 ± 0.001	49.5	62.8
^{165}Ho	0.600 ± 0.050	40.8	45.4
^{197}Au	128 ± 18	26.9	25.7

Barriers for hyper-fission

Table 1
The height of the inner and outer fission barriers for the ^{238}U and $^{239}_{\Lambda}$U nuclei when the Λ particle occupies the lowest single-particle state during fission.

	^{238}U	$^{239}_{\Lambda}$U
B_f (inner) (MeV)	8.20	8.47
B_f (outer) (MeV)	6.60	7.42

Fig. 1. The fission barrier of ^{238}U (the dotted line) and $^{239}_{\Lambda}$U (the solid line) nuclei obtained with the Skyrme–Hartree–Fock method. The Λ particle is assumed to occupy the lowest single-particle state during fission. The energy curves are shifted so that the ground state configuration has zero energy.
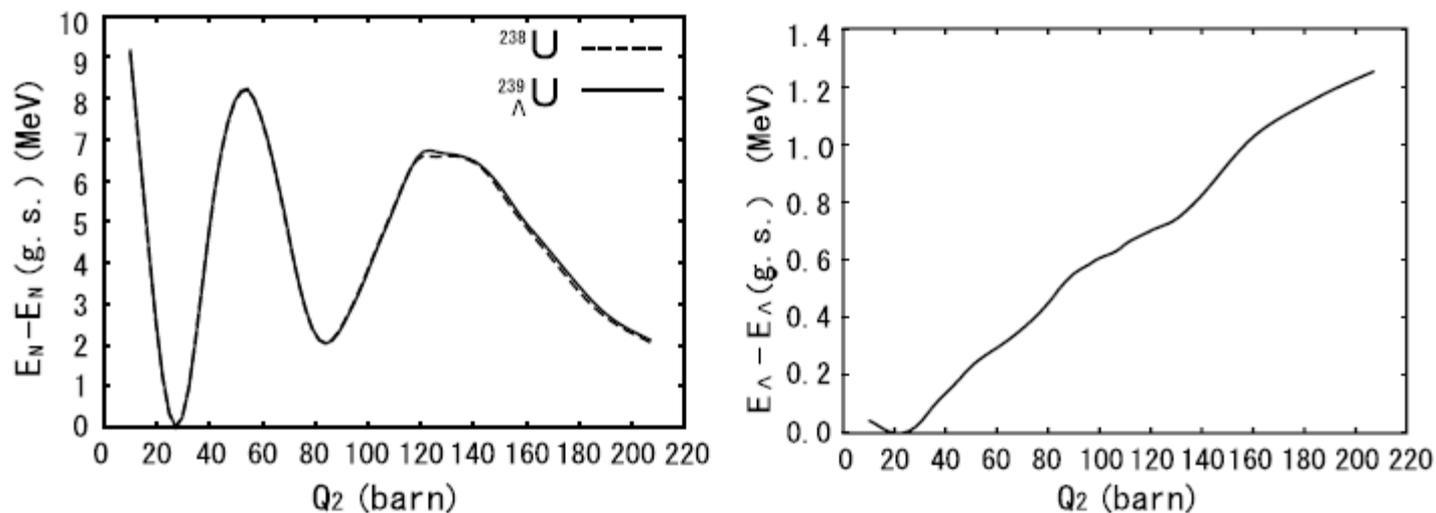

Fig. 2. (The left panel): The energy of the core nucleus E_N for the ^{238}U (the solid line) and $^{239}_{\Lambda}$U (the dashed line) nuclei as a function of the total quadrupole moment Q_2. The Λ particle is assumed to be at the lowest single-particle state. (The right panel): The energy of the Λ particle E_Λ for $^{239}_{\Lambda}$U with respect to that for the ground state as a function of Q_2.

Fission of heavy hypernuclei formed in antiproton annihilation

T.A. Armstrong et al., PRC 47 (1993) 1957

Heavy hypernuclei are produced in the annihilation of antiprotons in ^{238}U. The delayed fission of heavy hypernuclei and hypernuclei of fission fragments are observed by using the recoil-distance method in combination with measurement of secondary electron multiplicity. The lifetime of hypernuclei in the region of uranium is found to be $(1.25 \pm 0.15) \times 10^{-10}$ sec. It is observed that Λ hyperons predominantly stick to the heavier fission fragments. The yield of hypernuclei is found to be $(7.4 \pm 1.7) \times 10^{-3}$ per stopped antiproton. No coincidences with K^+ were found. Statistical and systematic errors on the number of events expected do not rule out this possibility.

The main results of the present experiment are the following. (i) The annihilation of antiprotons in ^{238}U leads to the production of hypernuclei of fission fragments and of heavy hypernuclei in the region of uranium. (ii) The lifetime of the heavy hypernuclei is found to be $(1.25 \pm 0.15) \times 10^{-10}$ sec. (iii) When the fission of an excited hypernucleus occurs, the Λ hyperon predominantly sticks to the heavy fragment; this fact can be used in the analysis of the dynamics of fission [17]. (iv) The probability of Λ-hyperon attachment to a heavy nucleus, following $\bar{p}$ annihilation, is estimated to be about 25%. (v) We do not find with significant confidence that K^+ are produced in coincidence with the hypernuclear events. However, this conclusion depends on complex and poorly known features of kaon production in heavy nuclei.
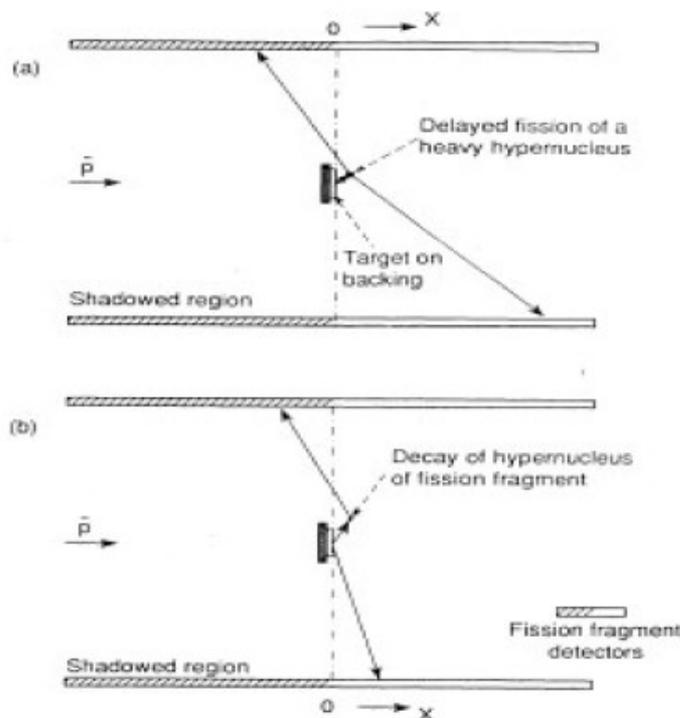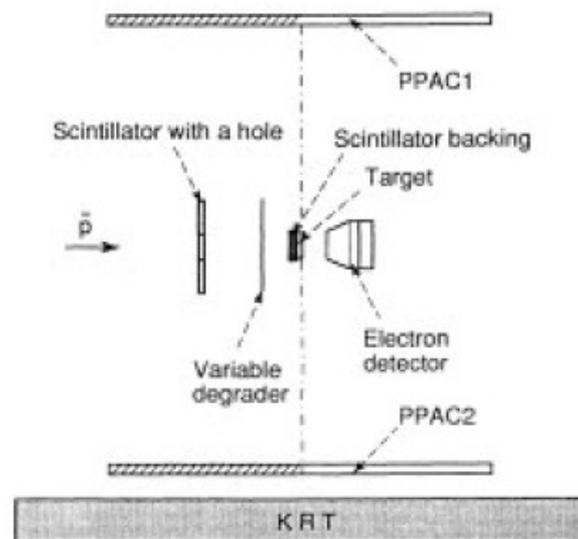

FIG. 1. Schematic representation of the recoil-distance method as applied to the study of (a) delayed fission of heavy hypernuclei, and (b) decay of hypernuclei of fission fragments. Both types of events can provide hits in the shadowed region (hatched) of the detectors while prompt fission cannot.

FIG. 2. Scheme of the experimental setup (not to scale). PPAC is the parallel plate avalanche counter; KRT is the Kaon range telescope.

Λ-hyperon lifetime in very heavy hypernuclei produced in the $p+$U interaction

The recoil shadow method for the detection of fission fragments has been used to investigate delayed fission of very heavy Λ hypernuclei produced in the p-U interaction at the projectile energy of 1.5 GeV. From the measured distribution of delayed fission events in the shadow region and the calculated momenta of hypernuclei leaving the target the lifetime of the Λ hyperon in very heavy hypernuclei was determined to be $\tau = 2.40 \pm 60$ ps. The comparison of the number of delayed fission events with that of the prompt events leads to an estimation of the cross section for the production of Λ hypernuclei in $p+$U collisions at 1.5 GeV of $\sigma_{Hv} = 150^{+150}_{-80}$ μb. [S0556-2813(97)04506-8]
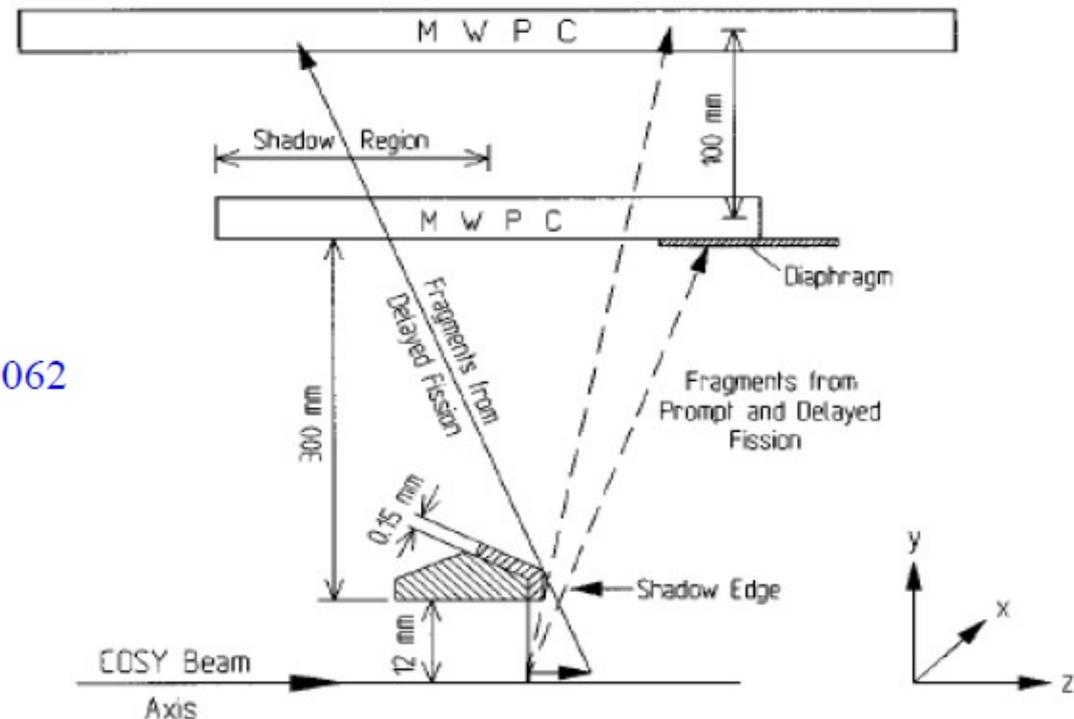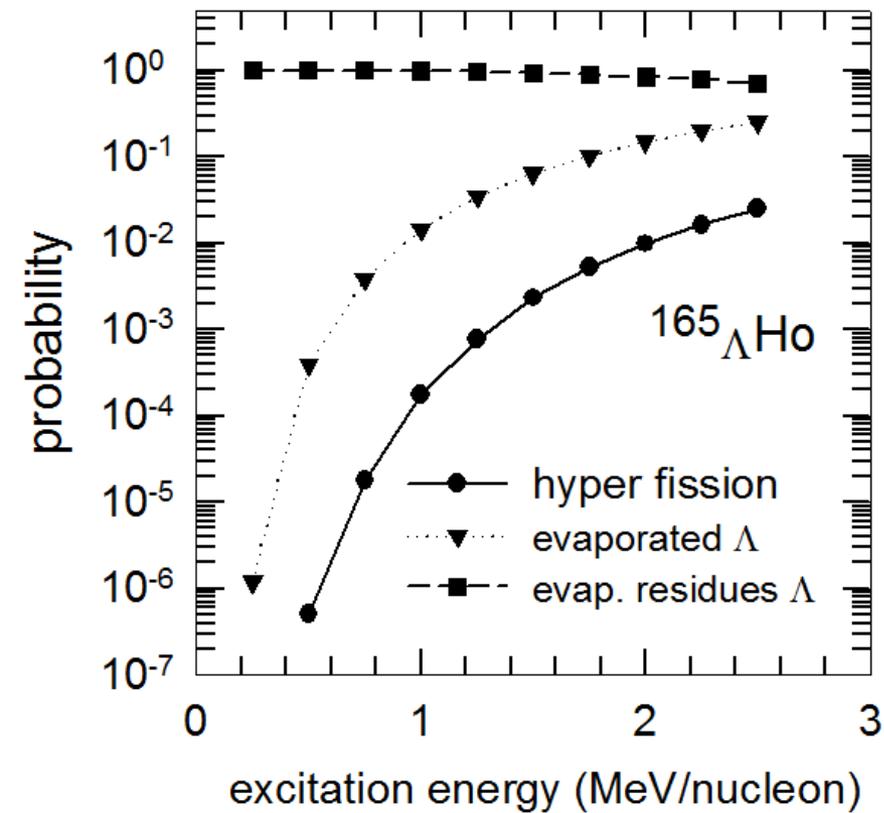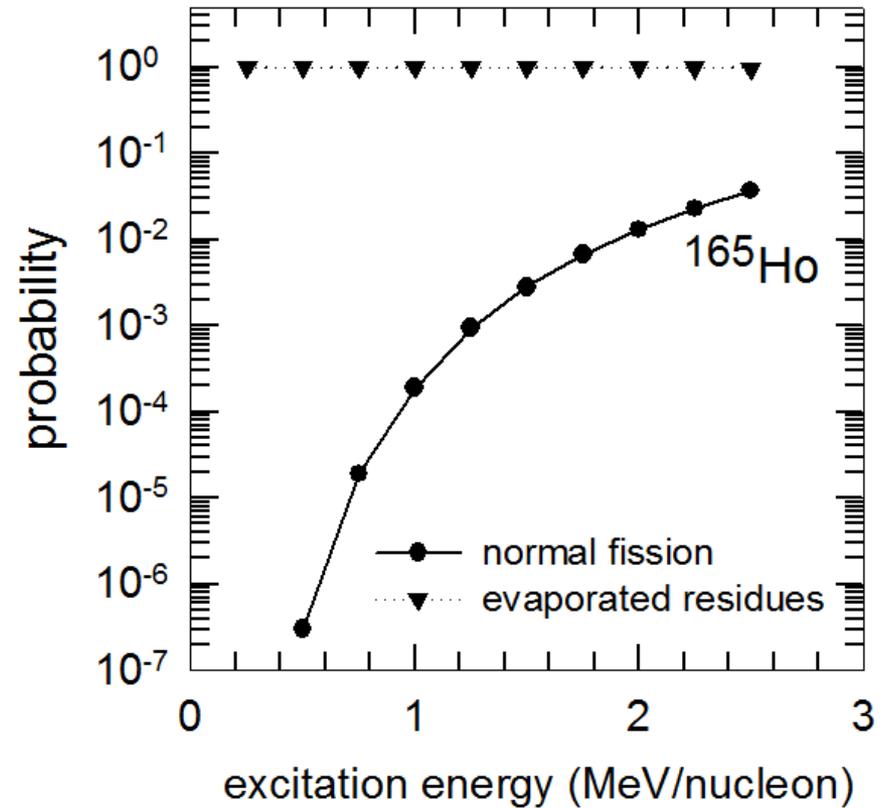
H. Ohm et al., PRC 55 (1997) 3062

FIG. 1. Schematic presentation of the experimental setup. The thickness of the target holder is enhanced in the drawing to show the details. The real distances are given.

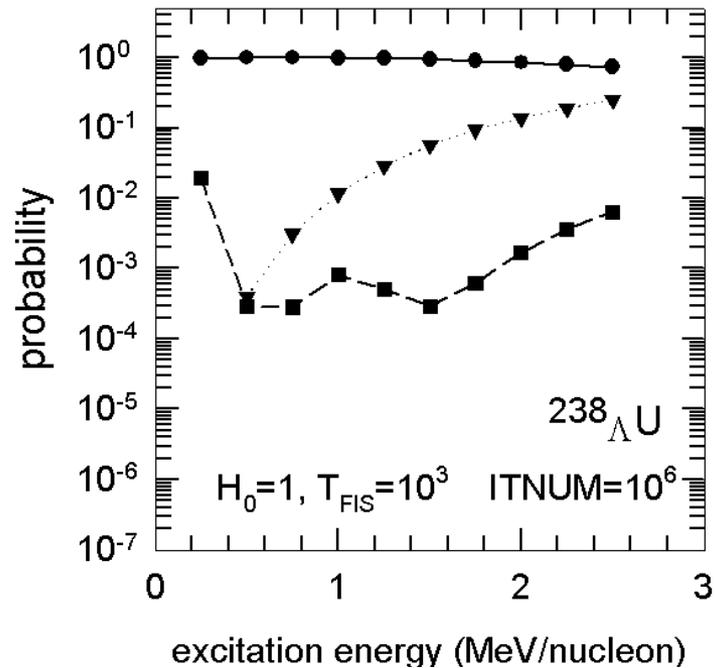# Statistical calculations of probabilities for fission and evaporation of heavy hypernuclei
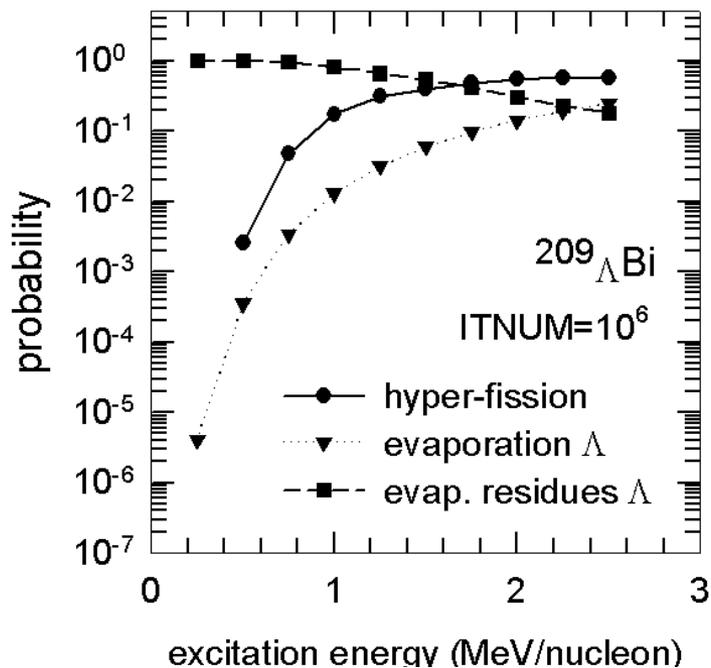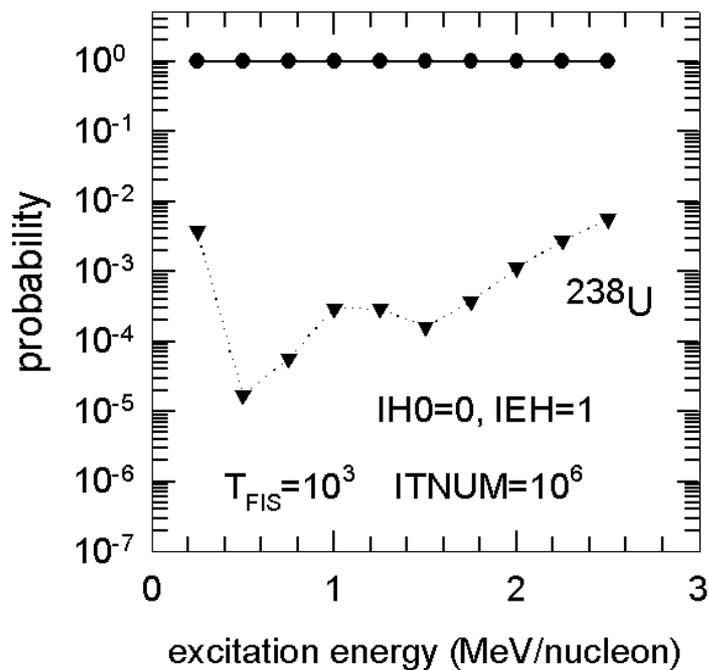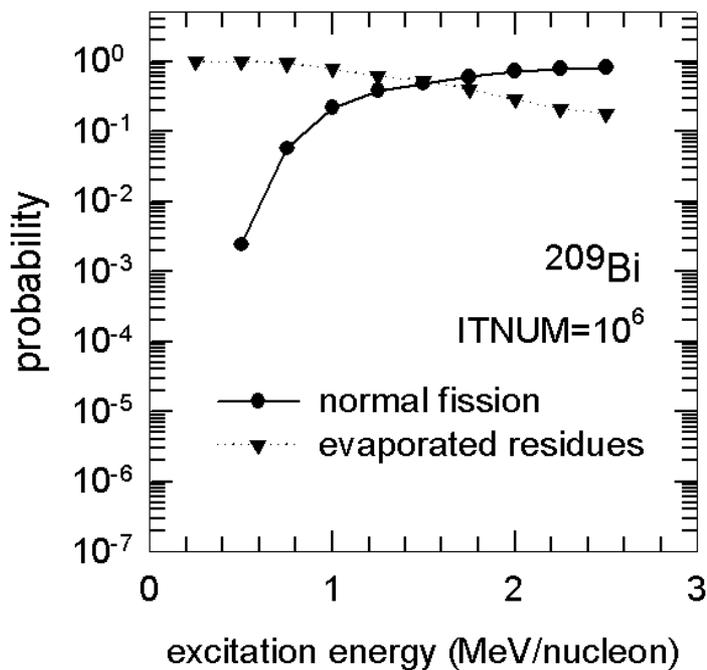

hyper   normal

hyper

normal

Nu ~ Nd ~ Ns

S=-∞

Strangeness in neutron stars (ρ > 3 - 4 ρ₀)
Strange hadronic matter (A → ∞)

p,n,Λ,Ξ⁰,Ξ⁻

higher density

ΛΛ, Ξ hypernuclei

ΛN interaction
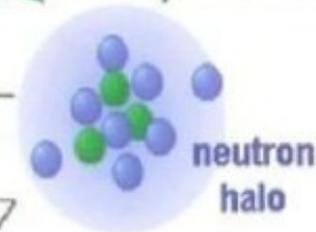
S=-2

Λ, Σ hypernuclei

Proton-rich nuclei

Strangeness

S=-1

Neutron-rich nuclei

Λ

proton number

non-strange nuclei

neutron halo

p   n

neutron number

3-dimensional nuclear chart

Conclusions

We have investigated the evaporation and fission of middle and heavy hypernuclei since they were not considered up to now because of scarce experimental data [H. Ohm et al., Phys. Rev. C 55, 3062 (1997)]. They should be dominating decay channels at low excitation energies. We are going to develop such models to use them also for the complementary study of producing exotic hypernuclei, e.g., neutron-rich and neutron-poor ones. Because of novelty of such processes there is an uncertainty in knowledge of level densities, shell corrections and some other parameters of hypernuclei.

In the beginning, the hypernuclear mass formulae obtained by Botvina-Pochodzalla (2007) is used. The level densities are calculated in the Fermi-gas approximation by taking into account protons, neutrons and hyperons, similar as it was done for normal nuclei. For the fission, we included the deformation of nuclear surface around the saddle point. We want to obtain a reasonable estimate of these decay channels in order to simulate future experiments.

We should emphasize that modification the parameters of the model in the presence of hyperons can be important for future comparison with experimental data.

In the future, we plan to analyze theoretically the formation of multi-hyperon nuclei, which can be abundantly produced in these reactions.

Our invetigations open the posibility to study formation of exotic hypernuclei (may be formed) via the secondary evaporation, fission, and multifragmentation-like processes.